Mitotic phosphotyrosine network analysis suggests a role for tyrosine phosphorylation in the regulation of Polo-like kinase 1 (PLK1)

Danielle Caron[1], Dominic P. Byrne[3], Philippe Thebault[1], Denis Soulet[4], Christian R. Landry[2], Patrick A. Eyers[3], and Sabine Elowe[1]

1 Department of Pediatrics, Faculty of Medicine, Université Laval, Centre Hospitalier Universitaire de Québec Research Center, Quebec City, QC G1V 4G2, Canada

2 Institut de Biologie Intégrative et des Systèmes (IBIS), Department of Biology, PROTEO, Université Laval, Pavillon Charles-Eugène-Marchand, 1030 Avenue de la Médecine, Quebec, QC, Canada, G1V 0A6.

3 Department of Biochemistry, Institute of Integrative Biology, University of Liverpool, Liverpool L69 7ZB, United Kingdom

4 Department of Psychiatry et Neurosciences, Faculty of Medicine, Université Laval, Centre Hospitalier Universitaire de Québec Research Center, Quebec City, QC G1V 4G2, Canada

Correspondence:

Sabine Elowe, Phone: (418) 654 2296, E-mail: sabine.elowe@crchudequebec.ulaval.ca

Running title:

The human mitotic tyrosine phosphorylation network

Key words: mitosis, phosphotyrosine, Plk1, tyrosine, phosphositeplus, phosphorylation

ABSTRACT

Tyrosine phosphorylation is closely associated with cell proliferation, and throughout the cell cycle phosphorylation events are most dynamic during mitosis. However, mitotic phosphotyrosine remains poorly characterized, despite numerous large-scale phosphoproteomic studies. This has resulted in significant gaps in our knowledge linking tyrosine phosphorylation with mitotic signaling events. Moreover, although few functionally-relevant mitotic phosphotyrosine sites have been characterized, recent evidence suggests that this modification may be more prevalent than previously appreciated. Here, we verified tyrosine phosphorylation in mitotic human cells at the spindle, spindle poles and at the plasma membrane. Database mining confirmed ~2000 mitotic phosphotyrosine sites and network analysis revealed a number of sub-networks that were enriched in tyrosine phosphorylated proteins including kinetochore and spindle components and SRC family kinases (SFKs). Polo-like kinase 1 (PLK1), a major signalling hub in the kinetochore/spindle sub-network, is phosphorylated at the highly conserved Tyr^{217} in the P+1 loop of the kinase domain. Substitution of Tyr^{217} with a phosphomimetic residue completely abrogated PLK1 activity, and subsequent phosphorylation of a physiological mitotic substrate. Strikingly, phosphorylation of Thr^{210} in the activation loop was negatively regulated by Tyr^{217} phosphorylation status. Our data support the idea that mitotic tyrosine phosphorylation may play a more prominent role than previously appreciated, as exemplified by our analysis of human PLK1.

INTRODUCTION

Throughout the cell cycle, phosphorylation events are thought to be most dynamic during mitosis (*1*), and seminal mitotic phosphoproteome studies have provided a wealth of data on serine (Ser) and threonine (Thr) phosphorylation (*2-13*). However, phosphotyrosine (pTyr) is comparatively rare, and is underrepresented and poorly annotated, even in datasets from large-scale mitosis-specific phosphoproteomic studies. Under basal conditions, and in the absence of specific signaling events, Tyr phosphorylation is maintained at sub-stoichiometric levels (*2*), presumably owing to the high activity of endogenous protein tyrosine phosphatases (*14, 15*). Consistently, phosphoamino acid and global phosphoproteomic analyses concur that protein phosphorylation occurs primarily at Ser and Thr residues (83% and 15% of sites, respectively) while Tyr phosphorylation represents only 0.5-2% of the total phosphoproteome (*16*). More recently, quantitative, high resolution and phosphoproteome-wide studies have identified a number of Tyr-phosphorylated peptides during mitosis, although they have received little attention in subsequent functional analyses (*2, 3, 5-13*). Despite this, evidence is accumulating that mitotic Tyr phosphorylation may be more prevalent and physiologically relevant than was previously appreciated.

The best understood pTyr site regulated during mitosis is arguably the inhibitory phosphorylation of cyclin-dependent kinase (CDK1) at Tyr^{15}, which is catalyzed by WEE1 and MYT1, and whose dephosphorylation serves as the basis for the switch-like activity of CDK1/cyclin B at mitotic entry [reviewed in (*17*)]. Interestingly, by exploiting the monoclonal 4G10 pTyr antibody, Tyr phosphorylation was originally detected at kinetochores and centrosomes in the mammalian PtK1 cell line over 20 years ago (*18*). More recent evidence in both meiotic and mitotic cells demonstrates that SRC family intracellular kinases (SFKs) are activated in mitosis, likely in a CDK1-dependent manner, and are then inactivated upon mitotic exit [reviewed in (*19*)]. SFKs are associated with, and activated at, the spindle and cortex during meiosis in mice, *Xenopus* and Zebrafish (*20-22*), and inhibition of

SFKs blocks meiotic progression (*23-25*), prevents the formation of microtubules, and reduces the amount of Tyr phosphorylated proteins in γ-tubulin complexes alongside disrupted spindle architecture. In mitosis, the SFK FYN co-localizes with the spindle and centrosomes in immune cells (*26*), and co-immunoprecipitates with γ-tubulin (*27*). More recently, inhibition of either SRC or the ABL tyrosine kinase was reported to induce spindle orientation and tilting defects in early prometaphase (*28, 29*), and FYN is also implicated in promoting spindle assembly and mitotic progression (*30*). Finally, activation of the cell surface EGFR has been shown to determine the timing of centrosome separation (*31*), and can selectively activate downstream signalling components, including SRC, during mitosis (*32*). Thus, while pTyr signalling appears relevant to spindle formation and function, the mitotic substrates and signalling pathways regulated by Tyr phosphorylation in human cells are not yet defined.

Here, we postulate that pTyr signaling in mitosis is more prevalent than previously appreciated, prompting us to identify and explore Tyr phosphorylation in the human mitotic phosphosignalling space. Our integrated approach revealed extensive Tyr phosphorylation during mitosis, particularly at the spindle and associated structures. Of particular interest, the key centrosome and kinetochore kinase PLK1 was found to be phosphorylated at Tyr^{217} in the P+1 loop of the kinase domain. Strikingly, substitution with a phosphomimetic amino acid completely abrogated PLK1 activity, and subsequent downstream PLK1 signaling. Although underrepresented and almost completely ignored in current models of mitotic phosphosignalling, our data indicate that tyrosine phosphorylation might play a more important biological role than previously appreciated, as exemplified by our analysis of PLK1.

RESULTS

Phosphotyrosine (pTyr) signals during mitosis.

To determine the relative extent of pTyr modification during the cell cycle, we ascertained global pTyr profiles by immunoblotting cell lysates synchronously progressing through the cell cycle with a pTyr specific antibody (4G10). Whereas basal pTyr signals did not change substantially between G1 and G2, a clear shift in the pTyr pattern was observed in mitotic cells (8h timepoint, fig. 1A). This was confirmed in cells that were artificially arrested in mitosis with the microtubule poisons nocodazole and taxol. This pattern was closely mimicked by two other pTyr antibodis, PY20 and pY100 (fig. S1A), verifying these findings.

We next evaluated the subcellular localization of pTyr signals during mitosis. Confocal imaging revealed robust pTyr staining along the cell perimeter and at pole-proximal regions of the spindle (fig. 1B, top panel). Identical staining patterns were observed with 2 independent pTyr antibodies (pY100 and 27B10, fig. S1B-C). To examine the specificity of the 4G10 antibody for immunofluorescence, cells were permeabilized and then treated with λ-phosphatase to induce de-phosphorylation prior to fixation and staining, which resulted in an almost complete loss of pTyr antibody signals (fig. 1B, bottom panel). As an additional control, the converse experiment was performed. To stimulate tyrosine phosphorylation, the activity of endogenous protein tyrosine phosphatases was inhibited using the potent pervanadate derivative bpV(phen). As expected, an overall increase of pTyr signal was observed in cells cultured with bpV(phen), including a significant ($p=0.026$, Mann Whitney t-test) increase of the pTyr signals that were directly associated with spindles (fig. 1C).

To further investigate pTyr at the spindle and associated structures, U2OS (fig. 1D) and HeLa (fig. S1D) cells were treated with DMSO (vehicle) or synchronized in mitosis with low doses of nocodazole and taxol before fixation and staining with pTyr antibodies. We found that a substantial amount of pTyr signal remained associated with the diminished spindle upon treatment with taxol and

nocodazole, as confirmed by quantitation of spindle-associated pTyr signals (fig.1D, middle and lower panels). Moreover, enhanced stabilization of the spindle with taxol appeared to significantly increase the associated pTyr signal ($p=0.0011$, one-way ANOVA, Dunnett's multiple comparison test, fig.1D, right), but no significant change was observed in nocodazole treated cells. A 3D reconstruction of pTyr staining of an intact spindle is shown in movie S1. Collectively, these observations support and extend previous observations (*18*), and demonstrate that a substantial amount of tyrosine phosphorylation in mitotic cells is concentrated at the cell cortex, around the centrosomes, as well as on the mitotic spindle.

Collation of mitotic and spindle-specific pTyr sites from phosphoproteomic studies.

The systematic identification and cataloguing of mitotic phosphorylation events from large scale proteomic studies has yielded remarkable insight into mitotic progression (*2, 3, 5-13*). However, these studies largely excluded pTyr sites from in-depth analysis. To explore these sites in a systematic manner, we used the PhosphoSitePlus database (PSP) (*33*) established by Cell Signalling Technologies (CST) to generate a dataset of tyrosine phosphorylated proteins (and annotated sites of phosphorylation) that were originally identified in disparate mitosis-specific, shotgun mass-spectrometry studies. The data curated by PSP employs a common standard of analysis for all sites, whether from publications or from CST experimental datasets, which permitted internal normalization of independent datasets. Importantly, only sites with localization scores of $P \leq 0.05$ or A-score > 13 qualified for inclusion in PSP, substantiating their inclusion.

The workflow for identifying mitotic pTyr sites is presented in fig. 2. Initially, all curated information from published mitotic studies (table S1 for the publication list) from HeLa cell extracts (including HeLa-S3) were collected. We focused on HeLa cells as they are the most commonly employed human model for studies of mitosis, especially phosphoproteomic dataset generation. Data

from a total of 104921 published phosphosites at the time of collation includes 1507 non-redundant pTyr-peptides from 1117 non-redundant proteins (table S2), representing 2% of phosphorylation sites. CST has independently identified pTyr sites from mitotically enriched Hela cells in a number of studies which have been also deposited in PSP (table S3). Using the same criteria as above, we probed the CST curation dataset in parallel, and identified an additional 596 non-redundant pTyr peptides derived from specific pTyr-enrichment approaches, which resulted in an 81% pTyr peptide content in these experiments (fig. 2A, table S4). A small number of pTyr sites (36) were identified from mitotic HeLa cells that were specifically enriched for pSer/Thr (tables S5, S6). Finally, the two datasets were merged to create a list of 1344 non-redundant proteins and a corresponding list of 1950 unique tyrosine phosphorylated peptides from mitotic cells (table S7). The curated and CST-generated datasets overlapped by 154 proteins which represents approximately 8% and 25% of each set, respectively (fig. 2B). Surprisingly, approximately 4% of total phosphosites identified in mitotic studies correspond to pTyr, which is somewhat larger than the predicted 0.5-2% ((*34*), fig. 2C). We suggest that this skew is likely introduced by pTyr enrichment approaches used in a number of the studies. Collectively, however, our analysis suggests that pTyr signalling may be much more prevalent during mitosis than previously thought.

Our immunofluorescence observations demonstrate marked tyrosine phosphorylation at the spindle, in agreement with previous studies (*18, 30*). By interrogating our final definitive dataset, we next searched for and annotated tyrosine phosphorylated proteins found at the spindle and associated structures. We first generated a list of spindle proteins from PSP associated with the search terms kinetochore, centrosome, spindle, centriole, centromere and pericentriolar material, thereafter referred to as “spindle proteins”. This resulted in total of 605 protein identifications, which were cross-referenced with our pTyr dataset to confirm mitotic tyrosine phosphorylation of 116 spindle proteins (8.6%) corresponding to 203 pTyr peptides (10.4%) (tables S8, S9, fig. 2D). This suggests that a

significant proportion of pTyr signalling occurs on proteins found at the mitotic spindle and associated structures.

Functional annotation of Mitotic pTyr network.

To elucidate the signaling networks and biological processes that are regulated by pTyr during mitosis, we performed network analysis of 1344 mitotic tyrosine-phosphorylated proteins. We first gathered protein-protein interaction data from the STRING (Search Tool for the Retrieval of Interacting Genes/Proteins) database (*35*) and then visualised them in Cytoscape (*36*). The resulting collated network is unexpectedly dense and highly inter-connected with 805 nodes and 4384 edges, although a number of outstanding nodes are also apparent (fig. S2A). GO analysis of the entire network revealed enrichment of proteins involved in processes such as phosphosignalling, cytoskeletal organization and chromosome organization, as expected (fig. S2B, C). We then analysed densely connected clusters within the network of protein interactions using MCODE (*37*), in order to highlight nodes predicted to be involved in specific cellular processes. This approach yielded four prominent clusters, termed Clusters 1 through 4 (fig. 3). Mapping of the 'spindle' network (yellow fill circles) onto the larger mitotic network (blue fill circles) confirmed the presence of a major spindle-associated subnetwork (Cluster 2), and also revealed the integration of known spindle proteins into other pTyr-containing clusters. As further described below, Gene ontology (GO) analysis of each of the four major clusters (table S10) indicated their enrichment in biological processes and cellular components (*38, 39*) .

Cluster 1 (fig. 3A) includes pTyr proteins implicated in the spliceosome, mRNA processing and splicing, and components of protein translation regulation. With the exception of a few exceptions (*40*), basic nucleolar functions such as splicing are thought to be shut down during mitosis, although this does not exclude a mitosis-specific regulatory role for some splicing factors, as has been recently

proposed (*40*). However, tyrosine phosphorylation of spliceosome and mRNA processing components has, to the best of our knowledge, not been previously recognised. This modification may be involved in inactivating the processing machinery during mitosis, or in regulating protein-protein interactions during splicing or spliceosome formation, as described for Ser/Thr phosphorylation (*41*).

Cluster 2 (fig. 3B) is highly enriched for pTyr-containing proteins involved in mitotic spindle organization. It includes proteins involved in spindle assembly (eg. centrosome associated proteins, KIF2B, and tubulin subunits) and proteins involved in centromere integrity and kinetochore assembly and function (eg. INCENP, SGO1, WAPL, CLASP2, CENPF, and CASC5/KNL1). Moreover, a number of mitotic Ser/Thr kinases with well-established roles in spindle assembly and regulation were enriched in this cluster. Interestingly, these included CDK1, Aurora A and B, and PLK1, a key regulator of mitosis (see below). With the exception of the inhibitory CDK1-pTyr^{15}, very little is known regarding the potential role of tyrosine phosphorylation for any of these mitotic kinases.

Cluster 3 (fig. 3C) is enriched in tyrosine kinases, including several members of the EphA receptor family, and rather conspicuously, non-receptor tyrosine kinases such as SFK members implicated in mitotic spindle dynamics (see discussion). Interestingly, this cluster also included the tyrosine phosphatase SHP-2 (ptpn11), which is known to be tyrosine phosphorylated and whose deficiency reportedly causes errors in kinetochore-microtubule attachments, chromosomal congression defects and missegregation, likely through inappropriate activation of PLK1 and Aurora B (reviewd in (*42*)).

Finally, Cluster 4 (fig. 3D) was enriched in proteins involved in glucose metabolism. These include the tumour-specific pyruvate kinase M2 (PKM2), which is instrumental in both aerobic glycolysis and gene transcription, and is also required for proper mitotic progression. Indeed, PKM2 specifically binds

to the spindle assembly checkpoint protein BUB3 and phosphorylates it at Tyr^{207} during mitosis (*43*). This phosphorylation is required for BUB3-BUB1 complex interaction with KNL1, and thus promotes kinetochore-loading of the checkpoint machinery, chromosome congression and the spindle assembly checkpoint. Strikingly, all three pTyr sites identified in PKM2 are in the protein kinase domain, suggesting that they may be directly involved in modulating PKM2 catalytic activity (*44*).

pTyr substrate motif and domain analysis.

To determine whether specific pTyr motifs are overrepresented in the mitotic pTyr dataset, and in an attempt to identify any conserved sequence motifs known to be recognized by protein-tyrosine kinases or protein-protein interaction domains, we performed motif analysis (*45*) on the 1950 mitotic and 203 spindle-associated pTyr sites. We exploited both the human IPI as a reference dataset to determine enrichment of the pTyr motifs in our dataset, and the entire pTyr cohort in PSP to specifically determine motif enrichment over and above global pTyr signalling; both approaches gave similar results (fig. 4A). Amongst the mitotic set, the most enriched motifs were pYXXSP and SPXpY motifs. The observed enrichment of (Ser/Thr) proline-directed phosphorylation motifs amongst our pTyr dataset is important, since a C-terminal Pro residue represents the minimal motif for phosphorylation of Ser/Thr by MAPKs and CDKs, including the master regulator of mitosis, CDK1. However, the observation that Tyr phosphorylation may occur in the vicinity of potential CDK sites has not previously been reported. Indeed, we found that in 46 of the 47 pYXXSP motifs, and in 34 of the 39 SPXpY motifs, the Ser residue was also reported to be phosphorylated in the PSP database.. Moreover, in 11 of 46 pYXXSP motifs and 6 of 34 sites where the phosphorylation was found on both Tyr and Ser residues, a doubly phosphorylated peptide was identified in the mitotic phosphoproteomics studies (table S11), suggesting a possible crosstalk between mitotic pSer-Pro and neighbouring pTyr residues in the same polypeptide. In addition, we found that both mitotic and (in particular) spindle-specific

pTyr sets were highly enriched for pYXXP. Interestingly, the SH2 domains of a number of proteins, including those of intracellular kinases such as SFKs and ABL all share a general preference for the pYXXP motif (*46*). A number of basophilic motifs also emerged from our analysis. In particular robust enrichment of a Lys at the +5 or +6 position (pYX_4K, pYX_5K) was observed in the spindle dataset. Notably, a recent report suggested that modified Lys residues tend to occur more frequently in the vicinity of phosphorylated residues and that this tendency was particularly strong for pTyr, suggesting that crosstalk between modified Lys and pTyr residues may be occurring in mitosis (*2*). Consistently, in the spindle dataset, for 11 of the 26 pYX_4K motifs, lysine modification was also reported in PSP, whereas this number dropped to 2/20 for the pYX_5K motif. Finally, the spindle set revealed >2.5 fold enrichment of phosphosites with a Gly at the -2 position (GXpY). This generic motif is thought to be phosphorylated by a number of distinct tyrosine kinases, including the InsR, IGF1R and SRC (*47, 48*). Collectively, our analysis identified novel pTyr motifs and a combinatorial pattern of phosphorylation in the mitotic phosphospace, suggesting that tyrosyl site modification may be guided by other mitotic inputs such as phosphorylation of SP motifs and/or covalent Lys modifications.

We next exploited NetworKIN (*49*) to evaluate potential kinase-substrate relationships in both the mitotic and the spindle datasets. For 954 phosphosites, we identified a potential kinase. In the mitotic dataset, we observed some enrichment of sites potentially phosphorylated by Abl kinase, Eph and EGF receptors (albeit with low counts), whereas enrichment of SFK sites was significantly higher (χ^2 test 3.8E-20, fig. 4B). A similar pattern was observed in the spindle-associated dataset (χ^2 test 8.4E-6, fig. 4C). These results support and extend previous observations suggesting mitotic activity of intracellular kinases, and a number of receptor tyrosine kinases. The enrichment of potential SFK and Abl sites above the background set is in line with previous observations implicating these kinases in mitotic regulation, in particular at the spindle (*50*).

Considering that target sites for the SFKs were considerably enriched in both the mitotic and spindle dataset, we next sought to determine whether pTyr signals associated with the spindle were sensitive to chemical SFK inhibition. We treated cells with the relatively specific SFK inhibitor PP2 before fixing and staining with anti-pTyr antibodies. Confocal imaging and volumetric quantitation of pTyr directly associated with the spindle revealed a significant reduction ($p=0.026$, unpaired t-test) in pTyr signals (fig. 4D), suggesting that SFKs, or other PP2-sensitive tyrosine kinases, phosphorylate one or more spindle associated proteins.

Phosphorylation within protein domains is known to regulate domain function, the best example being reversible phosphorylation within kinase domains (see for example (*51*)). We thus determined whether the mitotic/spindle pTyr sites collated in our study resided within or outside domains in their respective proteins. We established that in the mitotic dataset 47% of pTyr sites were within known domains, similar to the case when all pTyr sites in PSP were taken into consideration, where 50% were found to be in domains. We found that protein kinase domains were considerably more tyrosine phosphorylated when compared to other domains annotated in our dataset; 59/829 being found in domains are in protein kinase domains in the mitotic set *versus* 434/16858 for non-mitotic, χ^2 test, $p<0.0001$, fig. 4E, see table S12 for detail). In summary, our observations suggest that multiple tyrosine kinases, and in particular SFKs, are functionally active during mitosis and may contribute to accurate and timely progression, likely through phosphorylation of many of the proteins collated in this study. One such Tyr-phosphorylated target is the key mitotic master Ser/Thr kinase, PLK1.

Functional validation of PLK1 Tyr^{217} phosphorylation during mitosis.

Somewhat surprisingly, our data analysis revealed tyrosine phosphorylation within the catalytic domain as a common regulatory modification in a number of mitotic Ser/Thr kinases. We were particularly intrigued by PLK1 phosphorylation at Tyr^{217} (table S8 and (*5*). This position is highly conserved

amongst Ser/The kinases, and most other kinases have either a Phe or a Trp at this position suggesting that a bulky, aromatic residue at this position is likely essential for kinase activity (table S13) . To address this in the case of PLK1, we initially measured total tyrosine phosphorylation of PLK1 Y217F and a potential phosphomimetic mutant Y217E, and compared them with PLK1 wild-type and a catalytically inactive D194A mutant (hereafter referred to as kinase dead KD). Western blotting confirmed that pTyr levels on PLK1 were further enhanced by treatment with bpV(phen), and that basal pTyr levels were constant between PLK1 wild-type, KD, Y217F and Y217E, suggesting either that Tyr^{217} is one of several mitotic pTyr sites on PLK1, or alternatively, that Tyr^{217} phosphorylation occurs on a small subpopulation of PLK1 in the cell (fig. S3A). The P+1 loop is a critical point of interaction between the substrate and the kinase (*52*), and phosphorylation in the P+1 loop of several mitotic Ser/Thr kinases, including MPS1 (*53*) and BUB1 (*54*), has been shown to be important for modulation of their activity. We therefore measured the catalytic activity of Y217F and Y217E PLK1 mutants using ^{32}P-based kinase assays. Whereas Y217F retained significant kinase activity when compared side-by-side with PLK1, we were unable to detect activity in exogenous full-length PLK1 Y217E, suggesting that while a Phe at this position of the P+1 loop can be tolerated, the negative charge introduced by the Glu substitution completely abrogates catalytic activity (fig. 5A,B, $p=0.005$ for PLK1 autophosphorylation, randomized block Anova). Recent work shows that partial PLK1 activity is required to support proper spindle formation and mitotic progression through phosphorylation of a number of specific substrates at centrosomes and kinetochores (*55*-*58*). To confirm the effect of PLK1-Tyr^{217} substitutions on mitotic progression, we generated inducible isogenic stable cell lines expressing siRNA-resistant wild-type, KD, Y217F or Y217E PLK1 constructs (fig. S3B-D). Induction of exogenous PLK1 was coupled to siRNA depletion of endogenous PLK1 (fig. 5C). We next measured two different outputs of PLK1 function: mitotic progression and phosphorylation of a known PLK1 substrate. First, we determined mitotic arrest and progression, which

reflects a requirement for PLK1 in proper spindle assembly and functioning. As expected, PLK1 depletion in the parental cell line resulted in a significant increase in the percentage of cells arrested in mitosis from approximately 5% in control cells up to 49% after depletion, and this arrest was relieved by the re-expression of wild-type and Y217F PLK1 but not KD or Y217E mutants (fig. 5D, p=0.001, randomized block Anova). In agreement with this finding, quantification of mitotic stages demonstrated a significant number of cells arrested at prometaphase in PLK1-depleted cells and also in cells rescued with KD and Y217E PLK1 (fig. 5E p=0.0001, randomized block Anova). We next assayed the phosphorylation of the endogenous canonical PLK1 kinetochore substrate BUBR1 on Ser^{676} (*59*). As expected, BUBR1-Ser^{676} phosphorylation was abolished upon PLK1 depletion, but was restored by re-expression of wild-type and Y217F PLK1 but not KD or Y217E PLK1, and these changes were significant (fig. 5F, p=0.0001, heterogeneous one-way Anova). In agreement with these findings, a very recent report demonstrated that PLK1 Y217F expressing cells exhibited subtle mitotic defects that did not affect long term cell viability, in contrast to a kinase-dead PLK1 (*58*). Together, these observations suggest that introduction of a negative charge on Tyr^{217} through PLK1 phosphorylation might inactivate the kinase during mitosis.

We next sought to understand how Tyr^{217} phosphorylation might inhibit PLK1 activity mechanistically. First, we generated recombinant PLK1 kinase domain variants (Y217F, Y217E, and KD) in a T210D background, which mimics the activating phosphorylation generated by the Aurora kinases, locking PLK1 in an active conformation (fig. S4A). Measurement of thermal stability of wild-type and mutant PLK1 proteins using Differential Scanning Fluorimetry (DSF) indicated they were folded, and exhibited differential thermal stability with Y217E and Y217F markedly less stable than the T210D mutant in the absence of ligands (fig. S4B). In the presence of ligand, we found that PLK1 T210D, Y217E and PLK1 T210D,Y217F (but not PLK1 T210D,KD) bound to Mg:ATP complexes, as indicated by an increase in their thermal stability (fig. 6A). Furthermore, all four proteins interacted

strongly with the PLK1 inhibitor BI2536 and the broad spectrum kinase inhibitor staurosporine, but not the Aurora kinase inhibitor VX 680 (fig. 6A). This data collectively confirms that the ATP binding site is intact and accessible in these proteins, and that the loss of catalytic activity associated with Y217E is not likely due to an inability to bind ATP.

We next sought to determine whether any relationship might exist between multisite phosphorylation at Thr^{210} and Tyr^{217}. In agreement with kinase assays employing full-length PLK1 isolated from human cells, the recombinant PLK1 kinase domain was active if either Tyr or Phe was present at position 217, whereas Y217E PLK1 could not autophosphorylate, or phosphorylate α-casein, under identical conditions (fig. 6B). In addition, T210D or T210D, Y217F PLK1 phosphorylated an optimized peptide substrate with similar Km [ATP] values, suggesting functional equivalence, whereas PLK1 T210D, Y217E failed to detectably phosphorylate this peptide (fig.6C). This finding reveals that mimicking phosphorylation of Tyr^{217} with Glu inhibits kinase activity even in the presence of a hyperactivating, stoichiometric, T210D mutation. Next, we tested the potential for crosstalk between Thr^{210} and Tyr^{217}. To accomplish this, we generated PLK1 T210A, which abolished the constitutive negative charge stationed at this position in PLK1 T210D. Consistently, although PLK1 T210A was less active than PLK1 T210D, the activity of T210A,Y217F PLK1was further reduced when compared to T210D,Y217F PLK1, whereas Y217E PLK1 remained inactive regardless of the T210 status (fig. 6D, E, compare also fig. 6D to fig. 6B). Thus, a negative charge at Thr^{210} upon phosphorylation might be particularly important for catalytic activity in the context of PLK1 Y217F. Finally, to determine whether Tyr^{217} phosphorylation impacts upon Thr^{210} phosphorylation in cells, we measured the relative phosphorylation of Thr^{210}, confirming that whereas active PLK1 wild-type and Y217F were phosphorylated at low levels on Thr^{210}, KD and Y217E PLK1 exhibited much higher levels of Thr^{210} phosphorylation (fig. 6E), suggesting that Tyr^{217} phosphorylation may impact on activation segment

phosphorylation, which culminates in cellular Thr^{210} hyperphosphorylation as a response to Tyr-mediated blockade of substrate binding.

DISCUSSION

Tyrosine phosphorylation during mitosis was established over 30 years ago. SFKs, and more recently a number of other tyrosine kinases such as ABL, the EGFR, and the metabolic kinase PKM2 have all been reported to be active during mitosis (*32, 44, 50*). Nevertheless, only a handful of mitotic tyrosine phosphorylation sites have been studied to date, and the field is lacking a concerted dataset for analysis of mitotic pTyr dynamics. This is partly due to the low stoichiometry (approximately 10%) in the absence of direct stimulation, as well as the localized and temporal nature of the relatively small and but highly selective pool of tyrosine phosphorylated targets (*2*). Here, we have taken an integrated approach that includes bioinformatics, cell biology and biochemistry to explore the depth, and role, of pTyr-dependent signalling during mitosis. Our analysis reveals enrichment of pTyr-specific signals at the plasma membrane and, most importantly, around the mitotic spindle and centrosomes in HeLa cells, in agreement with earlier reports (*18, 30*). By exploiting the PSP database, we compiled a resource of 1950 unique pTyr sites in 1344 proteins identified in mitotic cells through large-scale phosphoproteomics studies. The specific and general dynamics of Tyr phosphorylation between interphase and mitosis currently remains unclear, but represents an important future goal for quantitiative phosphoproteomics approaches. Nevertheless, to the best of our knowledge, this work represents the first systematic compilation and analysis of pTyr signalling during mitosis, and therefore presents a valuable resource and rationale for further exploration of mitotic pTyr signalling.

Bioinformatic analysis of mitotic pTyr sites.

Network analysis of mitotic proteins containing Tyr phosphorylation sites revealed new and known biological processes and pathways that are likely to be regulated by tyrosine phosphorylation. For example, our analysis identified multiple tyrosine phosphorylation substrates in a subnetwork that

contains many of the known components of the mitotic spindle apparatus. In addition, we verified a subnetwork enriched for SFKs, which is in agreement with our pTyr motif analysis demonstrating strong enrichment of SH2 domain binding motifs and SFK target sites. The high number and relative proportion of sites predicted to be targeted by SFKs is not unexpected, because these kinases are functionally pleiotropic and involved in fundamental processes including mitosis and cytokinesis (*60*). In agreement with our bioinformatics analysis and our observations of spindle-specific pTyr signals that are lost upon chemical SFK inhibition, both SRC and FYN kinases are directly implicated in spindle function. In meiotic cells, activated SFKs are localized to the spindle microtubules (*20, 22*), whereas in somatic cells, FYN is reported to localize to these mitotic structures (*26*). SRC promotes proper spindle orientation in early prometaphase through centrosome- mediated aster formation (*28*), whereas FYN is necessary for spindle formation and kinetochore-fibre stability in a manner dependent on kinase activity (*30*). Very recently, and in agreement with our own observations of PP2-sensitive pTyr signals at the spindle, PP2 treatment was shown to decrease FYN-induced pTyr signals around the centrosome (*30*). SFKs may also regulate cytokinesis through modulation of the cleavage furrow and abscission. The hyperactive, oncogenic form of SRC induces delocalization of MKLP2, the chromosomal passenger complex and subsequently MKLP1, from the spindle midzone leading to cytokinesis failure (*61, 62*). Moreover, a recent computational analysis of experimentally derived phosphosites revealed that the pYXXP motif (which is highly enriched in our dataset) and its variations were found to be one of the most common pTyr motifs in the phosphospace (*63*), and are known to be targeted by ABL (*48*) and a number of SFKs. Nothwithstanding these studies, very little is known about SFK substrates in mitosis, and proteins within our network are attractive candidate substrates for these tyrosine kinases during mitosis, that will be explored in the future.

An interesting observation from our current analysis is the presence of pTyr sites alongside other potential sites of Ser/Thr or Lys covalent modification. Crosstalk between different types of PTMs is

an emerging theme in cell signalling and may well be a common concerted mechanism of protein regulation (*64*). In addition to the new pTyr motifs identified in the mitotic phosphospace, our data suggest the possibility of crosstalk between tyrosine phosphorylation and pSP (CDK) motifs as well as Lys modifications during mitosis. Previous work has demonstrated that pTyr is preferentially found close to modifiable Lys residues, and that the frequency of co-modification is inversely proportional to the distance between these PTMs (*2*). Consistently, our data reveals enrichment of Lys-containing motifs at sites between 5 and 6 amino acids C-terminal to pTyr (fig. 4). Whether Lys modifications can co-exist on the same proteoforms, representing a new form of regulatory switch, remains to be established. Although the biological significance of potential PTM crosstalk remains unclear in the context of pTyr, one attractive hypothesis is that it may be used to assign functional relevance to distinct modifications, potentially implicating co-occurance of phosphorylated (in the case of Ser) and acetylated/ubiquitylated residues (in the case of Lys) for the multi-site regulation of protein function (*65-67*). Along the same lines, it is attractive to speculate that the presence of pSP motifs in the vicinity of pTyr may guide modification of the latter residue in mitosis. In line with this, we observed that the vast majority of Ser residues within pYXXSP and SPXpY motifs are known to be phosphorylated in PSP, and in a number of cases, mass spectrometric evidence for the doubly phosphorylated peptide does indeed exist in mitotic samples.

Inhibitory phosphorylation of PLK1.

Phosphorylation in the activation segment of protein kinases is a common mechanism of kinase regulation. However, activation loop phosphorylation of many kinases generally induces activating structural changes by repositioning key structural elements that permit substrate and cofactor binding and efficient catalysis (*52*). Although no common mechanism has been proposed for negative regulation of protein-Ser/Thr kinases, phosphorylation of several of the CDKs within the subdomain I

GXGXXG motif at the Thr^{14} and Tyr^{15} (hCDK1 numbering) are known to be inhibitory (*68-70*), and acetylation of the ATP coordinating Lys has been shown to reduce the kinase activity of CDK9 (*71*). In this study, we establish for the first time that mimicking phosphorylation of PLK1 on Tyr^{217} in the P+1 loop completely inhibits detectable kinase activity, likely through inhibition of substrate binding, although we cannot formally rule out the effect is due to the Glu substitution rather than a phosphomimicking effect *per se* (*52*). Nevertheless, and in agreement with this assertion, neither Mg:ATP nor kinase inhibitor binding was affected in PLK1 Y217F and Y217E, whereas PLK1 autophosphorylation and in-trans α-casein protein phosphorylation were selectively abolished in the Y217E mutant. Further evidence from the literature demonstrates the relevance of modifications at this position. A recent report demonstrated very high conservation of PLK1 Tyr^{217} homologous residues amongst human Ser/Thr kinases (*72*). Indeed, Tyr is found at the position equivalent to PLK1 Tyr^{217} in 272 of the 393 'typical' human protein-serine/threonine kinases, and phosphorylation at this residue has been reported for a number of these (*72*). For example, phosphorylation of the DNA damage response kinase CHK2 at the homologous Tyr^{390} site is dramatically decreased after exposure to ionizing radiation, suggesting that phosphorylation at this site is likely to be inhibitory to enzyme activity (*73*). Moreover, phosphorylation of Tyr^{210} in the P+1 loop of ERK1 has recently been proposed to be important for proper conformation of the active site, and neither ERK1 Y210F nor Y210E mutants were phosphorylated at Thr^{202} and Tyr^{204} by MEK1 in vitro (*72*). Of particular interest, PLK4 has also been reported to be phosphorylated on Tyr^{177}, the equivalent P+1 loop residue [(*74*), McSkimming et al. in press]. Finally, it is noteworthy that a Tyr residue at the homologous position is not conserved in any of the human protein-Tyr kinases examined, perhaps to prevent non-specific inhibitory tyrosine autophosphorylation in the activation segment (*72*). Collectively, our data suggests that P+1 loop Tyr phosphorylation (or in other motifs essential for substrate phosphorylation) may serve as a selective mechanism for inhibition of protein-serine/threonine kinase activity, and may be more common than

previously appreciated. Indeed, we highlight phosphorylation of Tyr^{148} of Aurora A in our compiled dataset, situated just after the Gly-rich loop. This modification has very recently been shown to be catalyzed by Golgi-associated SRC, and appears to be required for targeting of Aurora A to the centrosome (*75*).

We were initially surprised to find that mimicking PLK1 Tyr^{217} phosphorylation was inhibitory, considering that this site was originally identified in phosphoproteomic studies of mitosis and considering the prominent role of PLK1 in mitosis. We believe that this site is unlikely to be an example of 'accidental' or 'non-functional' phosphorylation as has been noted with some pSer/Thr sites (*76*). As noted above, pTyr sites are stringently regulated and multiple identifications of this site have been reported in proteomic databases, suggesting that it is likely to be physiologically relevant. Moreover, Tyr residues at this position are phosphorylated (and relevant to catalysis) in other kinases. Lastly, inhibitory phosphorylation of the master mitotic regulator CDK1 at Tyr^{15} is also commonly observed in mitotic studies (*68-70*), suggesting that pools of inhibited mitotic kinases must exist.

Instead, we propose that phosphorylation at this site may occur at very low stoichiometry to control selected populations of PLK1, or may be a rapid mechanism to maintain balanced PLK1 activity during the stages of cell division. Unfortunately, we were unable to generate phosphospecific antibodies to Tyr^{217}, in line with a very low and localized stoichiometry, and consistent with complex multi-site phosphorylation in the PLK1 activation segement [55]. Glutamate mimicking of pTyr at this site did not support activity even in the background of the hyperactive PLK1 T210D, suggesting a dominant substrate blockade. This suggests complex structural and regulatory requirements for kinase activation/inactivation that extend beyond PLK1 T-loop Thr^{210} phosphorylation, and may explain the remarkable specificity of PLK1 towards its substrates despite its highly pleiotropic localization. A more complete understanding of PLK1 inhibitory phosphorylation during mitosis will require detailed quantitative and spatiotemporal investigation of Tyr^{217} phosphorylation during interphase and mitosis,

and identification of the kinase responsible for this modification. Initial experiments demonstrate that SRC is not likely to be a physiological PLK1 tyrosine kinase, since incubation of recombinant PLK1 with active SRC fails to induce marked phosphorylation or to directly modulate PLK1 activity *in vitro* (fig. S5).

In conclusion, our study represents a valuable new resource for researchers in the mitosis and tyrosine kinase signalling fields. We provide evidence that this modification may be much more important in mitosis than previously thought. Quantitative proteomics approaches are needed to establish how changes in pTyr that occur during mitosis (and in interphase) are specifically linked to the cell cycle. This will provide a more complete picture of the dynamic mitotic phosphoproteome and furnish researchers with substrates linked to cancer-associated tyrosine kinases.

METHODS

Cell culture

All cells were maintained in DMEM with high glucose (Dulbecco's modified Eagle's medium; HyClone) containing 10% BGS, 1% L-glutamine, 1% penicillin/streptomycin and cultured at 37°C in a 5% CO_2. For western blotting and immunofluorescence, cells were synchronized in mitosis after release from a thymidine-mediated G1/S arrest. For 293T cells, transfection was performed with 2µg/ml PEI and 300ng/ml of plasmid DNA. Depletion of endogenous PLK1 was performed using JetPrime at 2µl/ml (Polyplus) with 3.3µM DsiRNA (IDT) targeting a previously validated site (5'-CGAGCUGCUUAAUGACGAGUUCUTT-3')(*4*). DsiResistant PLK1 stable lines were generated by co-transfection of the pOG44 plasmid (Termo Fisher scientific) at 1.3µg/ml and pcDNA5/TO/FRT/ PLK1 wild-type and mutants (Thermo fisher Scientific) using Trans-IT LT-1 (Mirus Bio) at 3.5µl/ml. 48h post transfection, cells were trypsinized and cultivated in DMEM containing 10% BGS, 1% L-glutamine, 1% penicillin/streptomycin and 400µg/ml Hygromycin B. Clones were isolated after 3-4 weeks of selection and expression was verified by western blotting after induction with 50ng/ml of tetracycline (Sigma-Aldrich) for 24h.

Drug treatments and antibodies

Drug concentrations (unless otherwise indicated) were: 3.3 µM nocodazole (sigma), 200 nM paclitaxel (taxol, Millipore), 2mM thymidine (Thermo Fisher Scientific), all three for 16h; 20 µM PP2 (Abcam), and 20 µM Peroxovanadium derivative bpV(phen) (Calbiochem) .

The following antibodies were used in this study: anti-phosphotyrosine clone 4G10 (Millipore), clone PY20 (ENZO life sciences), clone pTY100 (CST), and clone 27B10 (Cytoskeleton, Inc.); anti-α-tubulin (11H10) Alexa®647 (CST), anti-γ-tubulin (Sigma-Aldrich), anti-MYC (9E10, Santa Cruz), anti-CENP-C (MBL international), anti-PLK1-pT210 (Rockland), anti-BubR1-pS676 (*59*). Anti-IgG

rabbit/mouse/guinea pig secondary antibodies for immunofluorescence and IgG horseradish peroxidase-conjugated secondary antibodies were purchased from Jackson ImmunoResearch.

Immunoblotting

Mitotic cells were collected by shake-off, rinsed in 1xPBS and directly lysed in RIPA buffer (10 mM Tris, pH 7.5, 150 mM NaCl, 1% NP-40, 10 mM NaF, 0,1% sodium deoxycholate, 1 mM sodium orthovanadate, 20 mM β-glycerophosphate, 10 mM sodium pyrophosphate, 10 μg/ml leupeptin, 10 μg/ml aprotinin, and 1mM AEBSF) under constant agitation for 30 min at 4°C before centrifugation (15 min, 20,000g) at 4°C. Protein concentrations of the clarified lysates were determined using the BCA assay (Pierce Thermo Fisher scientific), and equalized lysates were then resolved by SDS-PAGE and subsequent immunoblotting.

Immunofluorescence and volumetric quantification of pTyr signals by Imaris

Cells grown on coverslips were gently washed with TBS containing 100 μM sodium orthovanadate and then fixed and permeabilized simultaneously using PTEMF (0.2% Triton-X-100, 20 mM pipes pH 6.8, 1 mM $MgCl_2$, 10 mM EGTA, 4% formaldehyde) for 10 min. Cells were blocked (TBS 0.02% tween, 3% BSA, 100 μM Na_3VO_4) for 30 min, before staining with primary and secondry antibodies and mounting on slides using Fluoromount-G mounting media (Thermo Fisher scientific). Cells were imaged by confocal microscopy on an inverted Olympus IX80 microscope equipped with a WaveFX-Borealin-SC Yokagawa spinning disc (Quorum Technologies) and an Orca Flash4.0 camera (Hamamatsu). Image acquisition was performed using Metamorph software (Molecular Devices). Images were acquired by 0.5 μm z-steps at a depth of 5 μm using a 100× oil objective. Voxel size was 0.0529 x 0.0529 x 0.5 μm. Nine to twelve cells were imaged per experimental conditions. Three-dimensional reconstruction was performed using Imaris software (v 7.6.1, Bitplane). Briefly,

isosurfaces were generated in the surpass module to segment the α-tubulin structures as published previously(*77, 78*). The sum of intensities of pTyr signals was quantified within the segmented α-tubulin volume. Results are expressed as ratios of phosphotyrosine intensity per unit of volume of α-tubulin (μm^3).

Lambda-phosphatase assay

Cells grown on coverslips were rinsed with TM buffer (50 mM Tris pH 7.5, 5 mM $MgSO_4$). A 5 min extraction was realized using TM buffer with 1% CHAPS, 1 mM DTT and protease inhibitor cocktail. Cells were rinsed with TM buffer. Dephosphorylation was allowed for 10 min using TM buffer containing the λ-phosphatase, 1 mM DTT and the protease inhibitor cocktail. Cells were rinsed with TM buffer, incubated in TM buffer + 5 mM NEM for 5 min and rinsed again in TM buffer. Cells were then fixed using PTEMF and processed for immunofluorescence as describe earlier.

Kinase Assays

Mitotic cells were prepared in NP-40 lysis buffer (75mM Hepes pH7.5, 150mM KCl, 1.5mM EGTA, 10% Glycerol, 0.075% NP-40, 1 mM sodium orthovanadate, 20 mM β-glycerophosphate, 10 mM sodium pyrophosphate, 10 μg/ml leupeptin, 10 μg/ml aprotinin, and 1mM AEBSF) under constant agitation for 30 min at 4°C. Lysates were then centrifuged (15 min, 20,000g) at 4°C and protein concentrations were determined using the Bradford assay (Bio-Rad). Anti-MYC immunoprecipitations was performed on 500μg of protein with 10μl of protein G agarose (Thermo Fisher scientific) overnight at 4°C. Beads were washed 3x in lysis buffer and 1x in Kinase Reaction Buffer (50mM Tris-HCL pH7.5, 10mM β-Glycerophosphate, 100μM sodium orthovanadate). Samples were resuspended in 25 μl of KRB buffer complemented with 0.5mM DTT, 10mM $MgCl_2$, 50μM cold ATP, 5μCi of ^{32}P-ATP and 2μg/samples of casein (Sigma-Aldrich) before incubation for 30min at 30°C. Reactions were

stopped and samples were resolved by SDS-PAGE. Gels were stained with coomassie brilliant blue, destained and dried. Signals were revealed on BioMax MR-1 Film (Thermo Fisher scientific) and quantified in the linear range on ImageJ.

For protein substrate analysis with recombinant PLK1, 10 μg α-casein was incubated with 2 μg (~60 pmol) of wild-type, Y217E, and Y217F T210D or T210A PLK1 in 50 mM Tris, pH 7.4, 100 mM NaCl, 1 mM DTT and 100 mM imidazole at 30°C in the presence of 200 μM ATP (2 μCi ^{32}P ATP per assay) and 5 mM $MgCl_2$. At the indicated time points the reactions were terminated by denaturation after boiling in SDS sample buffer, prior to separation by SDS-PAGE and transfer to nitrocellulose membranes. ^{32}P-phosphotransfer to PLK1 and casein was detected by autoradiography, and the total amount of protein present in each lane was evaluated by Naphthalene blue staining of the membrane. To compare the specific activity of T210A and T210D PLK1 proteins, linear phosphate incorporation into PLK1 peptide was analysed using 1 μg of the appropriate protein in the presence of 25 mM HEPES, pH 7.4, 2μM PLK1 substrate peptide, 0.5 mM ATP, 5mM $MgCl_2$ and 1 mM DTT at 30°C. After 25 min, the extent of peptide phosphorylation was calculated by integrating the area under the phosphosubstrate peak, calculating percentage conversion and converting to pmoles phosphate transferred per minute of the reaction. The data shown represent the mean ± SD from two independent experiments carried out in duplicate.

PhosphoSitePlus dataset

Mitotic pTyr identifications from HeLa (and HeLa-S3) cells were downloaded from PSP. First, all curated information from published mitotic studies were downloaded and manually verified with the corresponding publication to only conserve the mitotic identifications adhering to the following criteria: FDR<1%, Ascore ≥13 and a localization probability ≥0.96. This corresponded to 1507 non-

redundant peptide related to 1117 non-redundant protein. Dataset from CST curation set corresponding only to mitotic extracts from HeLa cells (Tyr or Ser/Thr enriched and nocodazole treated) resulting to 596 non-redundant peptide corresponding to 408 non-redundant protein were also downloaded. These datasets were merged to create a master list of a uniformly non-redundant mitotic pTyr sites and proteins. The mitotic peptide list corresponds to all non-redundant pTyr sites based on their unique site group ID (according to PSP), with the exception of some isoform sharing the same group ID that were then sorted based on their unique peptide sequence. Next, all pTyr identifications from PSP associated with these GO term kinetochore, centrosome, spindle, centriole, centromere and pericentriolar material (including Subcellular Location, Biological Process, Molecular Function and Cellular Component; total 605 protein identification) were downloaded from PSP and cross-referenced with the mitotic list to confirm mitotic pTyr in 116 pTyr protein corresponding to 203 pTyr peptides named Spindle protein and peptide ID respectively. Finally, all pTyr peptide and protein identification (corresponding to 36176 peptides from 11959 proteins) on HeLa cells from PSP were downloaded and used as background information throughout bioinformatics analyses, unless otherwise stated.

pTyr Network Analyses

Functional and physical protein-protein interaction network were generated based on the Mitotic (1344 unique protein) and the Spindle (116 unique protein) protein list. The UniProtKB accession number corresponding to our Mitotic and Spindle PSP protein list were search against the STRING database version 10 for protein-protein interaction (Experimental and databases only, high confidence score 0.700) (*35*). The interactions were visualized on the Cytoscape platform ((*36*) version 3.2.0). Self-loops were removed and only interactions between the proteins belonging to the dataset were selected. The resulting interactome was analyzed for highly connected complexes with the theoretical clustering algorithm, Molecular COmplexe DEtection (MCODE) (*79*). The most highly-ranked sub-networks

were extracted for further analysis and rendering. Gene ontology (GO) term enrichment analyses were performed using the DAVID bioinformatics resources version 6.7 (medium stringency) (*80*). Functional clustering was performed using the following database: GO FAT, KEGG pathway, SMART, InterPro, Biocarta and Uniprot sequence feature. The statistical significance of the GO terms associated with Mitotic or Spindle protein ID was estimated by comparing it to our background (all pY from PSP). Kinase predictions were performed with NetworKIN (*49*) version 3.0 (kinomeXplorer) using the high throughput workflow option. A cut-off NetworKIN score of 1.5 was used. Phosphorylation motifs were extracted from pre-aligned tyrosine phosphorylated peptide using Motif-X version 1.2 (*45*). Analyses were performed with a significance cut-off of 0.001 and at least 20 occurrences of the motif in the dataset. Both the IPI human and complete PSP pTyr dataset were used as background data set with the built-in function, as indicated. Data on protein domains were obtained from http://pfam.xfam.org/proteome/9606#tabview=tab2 on June 11, 2015. The domains were parsed so that protein domains completely comprised within another one were eliminated, the longest being conserved. Each residue in the mitotic pTyr dataset was then assigned to a protein domain, if applicable.

Recombinant Protein Expression and Purification

Human PLK1 (1-369) T-loop mutants (T210D and T210A) were produced as *N*-terminal His6-tag fusion proteins in BL21 (DE3) pLysS *E. coli* (Novagen) and purified by immobilised metal affinity chromatography and gel filtration chromatography where appropriate (*81*). Y217E, Y217F and D194A point mutations were introduced by PCR-site directed mutagenesis as required in T210D and T210A backgrounds and purified as above. Proteins were ~80% pure prior to analysis, behaved as monomeric species after gel filtration, and were folded based on their thermal denaturation profiles.

PLK1 turnover analysed by microfluidic mobility shift assay using a fluorescent peptide substrate

To measure PLK1 peptide substrate phosphorylation, we developed a direct microfluidic phosphorylation-based assay, which permitted determination of a Km value for ATP. 1 μg of purified recombinant wild-type, Y217F or Y217E T201D PLK1 were assayed individually in the presence of the novel PLK1 fluorescent peptide substrate (5-FAM-AEEISDELMEFSLKDQEA-$CONH_2$, 5 μM) in the presence of the indicated concentrations of ATP and 5 mM $MgCl_2$. Peptide phosphorylation was calculated directly by measuring the conversion of the ratio of the peptide to the phosphopeptide after 1 h of assay at room temperature. Phosphate incorporation into the peptide was linear at this time point, and incorporation was limited to ~30% to prevent depletion of ATP at low concentrations. K_M [ATP] values were determined by non-linear regression analysis using Graphpad PRISM software.

Differential Scanning Fluorimetry (DSF)

Thermal shift assays were performed with a StepOnePlus RT-PCR machine (Life Technologies) employing a thermal ramp between 25 -95 °C (0.3 °C per data point). Thermal denaturation of purified PLK1 proteins (5 μM) was detected by the fluorescent emission of Sypro Orange dye (1:4000 final dilution). Assays included 1 mM ATP ± 10 mM $MgCl_2$ or the indicated concentrations of known PLK1 inhibitors (BI2536 and staurosporine) and a negative control compound (VX-680). For all assays, the final concentration of DMSO was 4%. Mean ΔTm values ± SD from duplicate experiments were calculated by subtracting the control Tm value (calculated using the Boltzmann equation) from the Tm value measure in the presence of ligand as described (*82*). Kinase inhibitor binding was evaluated as described previously (*83*).

SUPPLEMENTAL DATA:

Supplemental figures

Supplemental tables

Supplemental movies

Movie S1. 3D reconstruction of pTyr signals at the mitotic spindle.

REFERENCES and NOTES:

1. J. V. Olsen *et al.*, Quantitative phosphoproteomics reveals widespread full phosphorylation site occupancy during mitosis. *Science signaling* **3**, ra3 (2010).
2. K. Sharma *et al.*, Ultradeep human phosphoproteome reveals a distinct regulatory nature of Tyr and Ser/Thr-based signaling. *Cell Rep* **8**, 1583-1594 (2014).
3. R. C. C. Hengeveld *et al.*, Development of a Chemical Genetic Approach for Human Aurora B Kinase Identifies Novel Substrates of the Chromosomal Passenger Complex. *Molecular & Cellular Proteomics* **11**, 47-59 (2012).
4. A. Santamaria *et al.*, The Plk1-dependent phosphoproteome of the early mitotic spindle. *Molecular & cellular proteomics : MCP* **10**, M110 004457 (2011).
5. A. N. Kettenbach *et al.*, Quantitative phosphoproteomics identifies substrates and functional modules of Aurora and Polo-like kinase activities in mitotic cells. *Science signaling* **4**, rs5 (2011).
6. K. Grosstessner-Hain *et al.*, Quantitative Phospho-proteomics to Investigate the Polo-like Kinase 1-Dependent Phospho-proteome. *Molecular & Cellular Proteomics* **10**, (2011).
7. B. Hegemann *et al.*, Systematic phosphorylation analysis of human mitotic protein complexes. *Science signaling* **4**, (2011).
8. K. Nagano *et al.*, Phosphoproteomic analysis of distinct tumor cell lines in response to nocodazole treatment. *Proteomics* **9**, 2861-2874 (2009).
9. N. Dephoure *et al.*, A quantitative atlas of mitotic phosphorylation. *Proceedings of the National Academy of Sciences* **105**, 10762-10767 (2008).
10. R. Malik *et al.*, Quantitative Analysis of the Human Spindle Phosphoproteome at Distinct Mitotic Stages. *Journal of proteome research* **8**, 4553-4563 (2009).
11. M. Nousiainen, H. H. W. Silljé, G. Sauer, E. A. Nigg, R. Körner, Phosphoproteome analysis of the human mitotic spindle. *Proceedings of the National Academy of Sciences of the United States of America* **103**, 5391-5396 (2006).
12. H. Daub *et al.*, Kinase-Selective Enrichment Enables Quantitative Phosphoproteomics of the Kinome across the Cell Cycle. *Molecular cell* **31**, 438-448 (2008).
13. J. V. Olsen *et al.*, Quantitative Phosphoproteomics Reveals Widespread Full Phosphorylation Site Occupancy During Mitosis. *Science signaling* **3**, (2010).
14. H. Sun, N. K. Tonks, The coordinated action of protein tyrosine phosphatases and kinases in cell signaling. *Trends Biochem Sci* **19**, 480-485 (1994).
15. T. Hunter, Protein kinases and phosphatases: the yin and yang of protein phosphorylation and signaling. *Cell* **80**, 225-236 (1995).
16. J. V. Olsen *et al.*, Global, in vivo, and site-specific phosphorylation dynamics in signaling networks. *Cell* **127**, 635-648 (2006).
17. A. Lindqvist, V. Rodríguez-Bravo, R. H. H. Medema, The decision to enter mitosis: feedback and redundancy in the mitotic entry network. *The Journal of cell biology* **185**, 193-202 (2009).
18. S. Taagepera, M. S. Campbell, G. J. Gorbsky, Cell-cycle-regulated localization of tyrosine and threonine phosphoepitopes at the kinetochores of mitotic chromosomes. *Experimental cell research* **221**, 249-260 (1995).
19. R. Roskoski, Jr., Src kinase regulation by phosphorylation and dephosphorylation. *Biochemical and biophysical research communications* **331**, 1-14 (2005).

20. A. Talmor-Cohen, R. Tomashov-Matar, W. B. Tsai, W. H. Kinsey, R. Shalgi, Fyn kinase-tubulin interaction during meiosis of rat eggs. *Reproduction (Cambridge, England)* **128**, 387-393 (2004).
21. W. Wu, W. H. Kinsey, Role of PTPase(s) in regulating Fyn kinase at fertilization of the zebrafish egg. *Developmental biology* **247**, 286-294 (2002).
22. L. K. McGinnis, D. F. Albertini, W. H. Kinsey, Localized activation of Src-family protein kinases in the mouse egg. *Developmental biology* **306**, 241-254 (2007).
23. M. Levi, B. Maro, R. Shalgi, Fyn kinase is involved in cleavage furrow ingression during meiosis and mitosis. *Reproduction (Cambridge, England)* **140**, 827-834 (2010).
24. M. Levi, B. Maro, R. Shalgi, The involvement of Fyn kinase in resumption of the first meiotic division in mouse oocytes. *Cell cycle (Georgetown, Tex.)* **9**, 1577-1589 (2010).
25. M. Levi, L. Ninio-Mani, R. Shalgi, Src protein kinases in mouse and rat oocytes and embryos. *Results and problems in cell differentiation* **55**, 93-106 (2012).
26. S. C. Ley, M. Marsh, C. R. Bebbington, K. Proudfoot, P. Jordan, Distinct intracellular localization of Lck and Fyn protein tyrosine kinases in human T lymphocytes. *The Journal of cell biology* **125**, 639-649 (1994).
27. V. Sulimenko *et al.*, Regulation of microtubule formation in activated mast cells by complexes of gamma-tubulin with Fyn and Syk kinases. *Journal of immunology (Baltimore, Md. : 1950)* **176**, 7243-7253 (2006).
28. Y. Nakayama *et al.*, c-Src but not Fyn promotes proper spindle orientation in early prometaphase. *The Journal of biological chemistry* **287**, 24905-24915 (2012).
29. R. A. Klinghoffer, C. Sachsenmaier, J. A. Cooper, P. Soriano, Src family kinases are required for integrin but not PDGFR signal transduction. *The EMBO journal* **18**, 2459-2471 (1999).
30. M. Okamoto *et al.*, Fyn Accelerates M Phase Progression by Promoting the Assembly of Mitotic Spindle Microtubules. *Journal of Cellular Biochemistry* **117**, 894-903 (2016).
31. B. R. Mardin *et al.*, EGF-induced centrosome separation promotes mitotic progression and cell survival. *Developmental cell* **25**, 229-240 (2013).
32. P. Wee, H. Shi, J. Jiang, Y. Wang, Z. Wang, EGF stimulates the activation of EGF receptors and the selective activation of major signaling pathways during mitosis. *Cellular signalling* **27**, 638-651 (2015).
33. P. V. Hornbeck *et al.*, PhosphoSitePlus, 2014: mutations, PTMs and recalibrations. *Nucleic Acids Research* **43**, (2015).
34. T. Hunter, B. M. Sefton, Transforming gene product of Rous sarcoma virus phosphorylates tyrosine. *Proceedings of the National Academy of Sciences of the United States of America* **77**, 1311-1315 (1980).
35. D. Szklarczyk *et al.*, STRING v10: protein–protein interaction networks, integrated over the tree of life. *Nucleic Acids Research* **43**, (2014).
36. P. Shannon *et al.*, Cytoscape: a software environment for integrated models of biomolecular interaction networks. *Genome research* **13**, 2498-2504 (2003).
37. G. D. Bader, C. W. Hogue, An automated method for finding molecular complexes in large protein interaction networks. *BMC Bioinformatics* **4**, 2 (2003).
38. W. Huang da, B. T. Sherman, R. A. Lempicki, Systematic and integrative analysis of large gene lists using DAVID bioinformatics resources. *Nat Protoc* **4**, 44-57 (2009).
39. W. Huang da, B. T. Sherman, R. A. Lempicki, Bioinformatics enrichment tools: paths toward the comprehensive functional analysis of large gene lists. *Nucleic Acids Res* **37**, 1-13 (2009).

40. J. C. Hofmann, A. Husedzinovic, O. J. Gruss, The function of spliceosome components in open mitosis. *Nucleus (Austin, Tex.)* **1**, 447-459 (2010).
41. J. E. Mermoud, P. T. Cohen, A. I. Lamond, Regulation of mammalian spliceosome assembly by a protein phosphorylation mechanism. *The EMBO journal* **13**, 5679-5688 (1994).
42. G. Chan, D. Kalaitzidis, B. G. Neel, The tyrosine phosphatase Shp2 (PTPN11) in cancer. *Cancer Metastasis Rev* **27**, 179-192 (2008).
43. Y. Jiang *et al.*, PKM2 regulates chromosome segregation and mitosis progression of tumor cells. *Molecular cell* **53**, 75-87 (2014).
44. T. Hitosugi *et al.*, Tyrosine Phosphorylation Inhibits PKM2 to Promote the Warburg Effect and Tumor Growth. *Science signaling* **2**, (2009).
45. D. Schwartz, S. P. Gygi, An iterative statistical approach to the identification of protein phosphorylation motifs from large-scale data sets. *Nature biotechnology* **23**, 1391-1398 (2005).
46. B. A. Liu, B. W. Engelmann, P. D. Nash, The language of SH2 domain interactions defines phosphotyrosine-mediated signal transduction. *FEBS letters* **586**, 2597-2605 (2012).
47. R. Amanchy *et al.*, A curated compendium of phosphorylation motifs. *Nature biotechnology* **25**, 285-286 (2007).
48. K. T. S. Prasad *et al.*, Human Protein Reference Database—2009 update. *Nucleic Acids Research* **37**, (2009).
49. H. Horn *et al.*, KinomeXplorer: an integrated platform for kinome biology studies. *Nat Methods* **11**, 603-604 (2014).
50. S. Matsumura *et al.*, ABL1 regulates spindle orientation in adherent cells and mammalian skin. *Nature communications* **3**, 626 (2012).
51. L. L. Jin *et al.*, Tyrosine phosphorylation of the Lyn Src homology 2 (SH2) domain modulates its binding affinity and specificity. *Molecular & cellular proteomics : MCP* **14**, 695-706 (2015).
52. B. Nolen, S. Taylor, G. Ghosh, Regulation of protein kinases; controlling activity through activation segment conformation. *Molecular cell* **15**, 661-675 (2004).
53. R. K. Tyler *et al.*, Phosphoregulation of human Mps1 kinase. *Biochemical Journal* **417**, 173-184 (2009).
54. Z. Lin, L. Jia, D. R. Tomchick, X. Luo, H. Yu, Substrate-Specific Activation of the Mitotic Kinase Bub1 through Intramolecular Autophosphorylation and Kinetochore Targeting. *Structure* **22**, 1616-1627 (2014).
55. R. F. Lera, M. E. Burkard, High mitotic activity of Polo-like kinase 1 is required for chromosome segregation and genomic integrity in human epithelial cells. *The Journal of biological chemistry* **287**, 42812-42825 (2012).
56. M. E. Burkard *et al.*, Chemical genetics reveals the requirement for Polo-like kinase 1 activity in positioning RhoA and triggering cytokinesis in human cells. *Proceedings of the National Academy of Sciences of the United States of America* **104**, 4383-4388 (2007).
57. X. Liu, M. Lei, R. L. Erikson, Normal cells, but not cancer cells, survive severe Plk1 depletion. *Molecular and cellular biology* **26**, 2093-2108 (2006).
58. A. L. Lasek, B. M. McPherson, N. G. Trueman, M. E. Burkard, The Functional Significance of Posttranslational Modifications on Polo-Like Kinase 1 Revealed by Chemical Genetic Complementation. *PloS one* **11**, (2016).
59. S. Elowe, S. Hummer, A. Uldschmid, X. Li, E. A. Nigg, Tension-sensitive Plk1 phosphorylation on BubR1 regulates the stability of kinetochore microtubule interactions. *Genes & development* **21**, 2205-2219 (2007).

60. S. M. Thomas, J. S. Brugge, Cellular functions regulated by Src family kinases. *Annual review of cell and developmental biology* **13**, 513-609 (1997).
61. Y. Lee *et al.*, UNC119a bridges the transmission of Fyn signals to Rab11, leading to the completion of cytokinesis. *Cell cycle (Georgetown, Tex.)* **12**, 1303-1315 (2013).
62. S. Soeda *et al.*, v-Src causes delocalization of Mklp1, Aurora B, and INCENP from the spindle midzone during cytokinesis failure. *Experimental cell research* **319**, 13821397 (2013).
63. R. Amanchy, Identification of Novel Phosphorylation Motifs Through an Integrative Computational and Experimental Analysis of the Human Phosphoproteome. *Journal of Proteomics & Bioinformatics* **04**, (2011).
64. T. Hunter, The age of crosstalk: phosphorylation, ubiquitination, and beyond. *Molecular cell* **28**, 730-738 (2007).
65. P. Beltrao, P. Bork, N. J. Krogan, V. van Noort, Evolution and functional cross-talk of protein post-translational modifications. *Molecular systems biology* **9**, 714 (2013).
66. D. L. Swaney *et al.*, Global analysis of phosphorylation and ubiquitylation cross-talk in protein degradation. *Nature methods* **10**, 676-682 (2013).
67. P. Beltrao *et al.*, Systematic functional prioritization of protein posttranslational modifications. *Cell* **150**, 413-425 (2012).
68. J. P. I. Welburn *et al.*, How Tyrosine 15 Phosphorylation Inhibits the Activity of Cyclin-dependent Kinase 2-Cyclin A. *Journal of Biological Chemistry* **282**, 3173-3181 (2007).
69. Y. Gu, J. Rosenblatt, D. O. Morgan, Cell cycle regulation of CDK2 activity by phosphorylation of Thr160 and Tyr15. *The EMBO journal* **11**, 3995-4005 (1992).
70. P. R. Mueller, T. R. Coleman, A. Kumagai, W. G. Dunphy, Myt1: a membrane-associated inhibitory kinase that phosphorylates Cdc2 on both threonine-14 and tyrosine-15. *Science (New York, N.Y.)* **270**, 86-90 (1995).
71. A. Sabò, M. Lusic, A. Cereseto, M. Giacca, Acetylation of conserved lysines in the catalytic core of cyclin-dependent kinase 9 inhibits kinase activity and regulates transcription. *Molecular and cellular biology* **28**, 2201-2212 (2008).
72. S. Lai, S. Pelech, Regulatory roles of conserved phosphorylation sites in the activation T-loop of the MAP kinase ERK1. *Mol Biol Cell* **27**, 1040-1050 (2016).
73. X. Guo *et al.*, Interdependent Phosphorylation within the Kinase Domain T-loop Regulates CHK2 Activity. *Journal of Biological Chemistry* **285**, 33348-33357 (2010).
74. A. Shrestha, G. Hamilton, E. O'Neill, S. Knapp, J. M. Elkins, Analysis of conditions affecting auto-phosphorylation of human kinases during expression in bacteria. *Protein Expression and Purification* **81**, 136-143 (2012).
75. M. L. Barretta *et al.*, Aurora-A recruitment and centrosomal maturation are regulated by a Golgi-activated pool of Src during G2. *Nature communications* **7**, 11727 (2016).
76. C. R. Landry, E. D. Levy, S. W. Michnick, Weak functional constraints on phosphoproteomes. *Trends in Genetics* **25**, 193-197 (2009).
77. M. Cote, J. Drouin-Ouellet, F. Cicchetti, D. Soulet, The critical role of the MyD88-dependent pathway in non-CNS MPTP-mediated toxicity. *Brain Behav Immun* **25**, 1143-1152 (2011).
78. J. Piao *et al.*, Human Embryonic Stem Cell-Derived Oligodendrocyte Progenitors Remyelinate the Brain and Rescue Behavioral Deficits following Radiation. *Cell stem cell* **16**, 198-210 (2015).
79. G. D. Bader, C. W. V. Hogue, An automated method for finding molecular complexes in large protein interaction networks. *BMC bioinformatics* **4**, 1 (2003).
80. W. Huang da *et al.*, DAVID gene ID conversion tool. *Bioinformation* **2**, 428-430 (2008).

81. P. J. Scutt *et al.*, Discovery and exploitation of inhibitor-resistant aurora and polo kinase mutants for the analysis of mitotic networks. *The Journal of biological chemistry* **284**, 15880-15893 (2009).
82. J. M. Murphy, Q. Zhang, S. N. Young, M. L. Reese, A robust methodology to subclassify pseudokinases based on their nucleotide-binding properties. *Biochemical …*, (2014).
83. S. Mohanty *et al.*, Hydrophobic Core Variations Provide a Structural Framework for Tyrosine Kinase Evolution and Functional Specialization. *PLOS Genetics* **12**, (2016).

Acknowledgements: We would like to thank Rainer Malik and members of the Elowe Lab for helpful discussions. We also thank Mr. Gaétan Daiglefor guidance with statistical analyses.

Funding: Research in SE's lab is funded by grants for the Canadian Institutes for Health Research (CIHR, # 244442), the National Science and engineering research council (05841) and the Canadian Cancer Society (19140). SE is a CIHR New investigator. PAE acknowledges funding from the North West Cancer Development Fund and project grant CR1088. CRL's research is funded by grants 299432 and 324265 from CIHR and he holds the Canada Research Chair in Cell and Systems Biology.

Author contributions: DC, CL, and SE performed the datamining and bioinformatics analysis. DC and PT performed all immunofluorescence and Western blotting experiments, and IMARIS quantitation by DS. DB performed in vitro PLK1 assaysSE wrote the manuscript with help from DC and PAE. **Competing interests:** The authors declare no competing interests

Fig 1. Spindle specific pTyr signals during mitosis. (A) Immunoblot detection of pTyr using 4G10 antibody (top blot) on lysates arrested at different stages of the cell cycle. Extracts were prepared from asynchronous cells (Asynch), serum-starved cells presumably in G0, thymidine-arrested cells presumably in G1/S [0 hours (0h)], cells released for the indicated time until mitosis (10h), and nocodazole (N) or taxol (T)- arrested cells. Membranes were reprobed for cyclin B (middle blot) and α–tubulin (bottom blot). Blot is representative of 3 independent experiments. Bottom panel shows intensity profile plot for the Asynch and 10h lanes. **(B)** Cells were permeabilized and incubated with λ-phosphatase (λ-PPase) or control buffer (CNTL), fixed and stained with pTyr antibody 4G10 (red), γ-tubulin antibody (green), and α-tubulin antibody (blueBottom panl shows interphase cells from the same experiments.). Scale bar, 5 μm. **(C)** Cells were treated with 20 μM bpV(phen) for 10 minutes prior to fixation and stained with 4G10 (red), α-tubulin antibody (green), and DAPI (blue). Quantitation of the spindle-specific 4G10 staining is shown on the right. Scale bar, 5 μm. * represents $p < 0.05$. **(D)** U20S cells were treated with DMSO, nocodazole (10 ng/ml) or taxol (20nM) before being fixed and stained with anti-pTyr (4G10, red), anti-γ-tubulin (green), and anti-α-tubulin (blue). The final panel shows an enlargement of the volumetric rendering of the mitotic spindle (blue), the spindle poles (green) and pTyr (red). Quantitation of the spindle-specific 4G10 staining is shown for the different conditions. Data are mean ± S.E. of 10-15 cells from 1 experiment N= 3 independent experiments. ** represents $p < 0.01$.

Fig 2. Workflow of the mitotic tyrosine phosphorylation dataset construction. (A) Mitotic dataset information corresponding to pTyr identifications related to HeLa cells downloaded from PhoshoSitePlus. (**B)** Venn diagram of mitotic pTyr site overlap between published and CST curated

phosphorylation according to PSP. (**C)** Phosphorylation site distribution from mitotic HeLa studies in PSP. (**D)** Cross-reference between non-redundant mitotic pTyr protein identification found in PSP and the spindle protein identification responding to spindle associated definition according to PSP. For (B)-(D), the total number of sites per catagory are indicated in brackets. Figures discussed in the text are highlighted in grey.

Fig 3. Protein-protein interaction subnetworks. Subnetworks depicting the connectivity of highly connected clusters in the protein-protein interaction network from pTyr sites characterized in this study. The pTyr mitotic protein interaction network was determined in STRING and the highest ranking clusters [(A)-(D), MCODE scores indicated] were identified using MCODE plugin in cytoscape. Proteins within the spindle network are marked in yellow. Other key proteins are marked according to the legend. Node size represents the number of pTyr sites identified on the protein.

Fig 4. Motif and NetworKIN analysis of mitotic pTyr sites. (A) Enriched phosphorylation site motifs of phosphopeptides identified in both mitotic and spindle networks using the entire human proteome as a the reference dataset (left panels) and using the entire pTyr cohort reported in PSP as the reference dataset (right panels). **(B)** NetworKIN identification of kinase-substrate relationships for the mitotic networks. (**C),** As in (B) but for spindle networks. For the most common kinase identifications, the observed and expected hits are indicated. (**D)** HeLa cells were treated with DMSO or 20 μM PP2 for 30 minutes before fixation and staining with pTyr antibody (4G10 , red), anti-γ-tubulin antibody (green), and anti-α-tubulin antibody (blue). Scale bar ,5 μm. Volumetric quantitation of pTyr signal intensity from 12-15 cells directly associated with the spindle is indicated on the graph. Data are mean

± SE of 9-13 cells from 1 representative experiment, N=3 independent experiment. (**E)** Percentage of pTyr sites observed and expected within individual domains.

Fig 5. **Characterization of the effect of PLK1 Tyr^{217} phosphorylation.** . **(A)** In vitro kinase assay of full length PLK1 wild-type, KD, the Y217F and Y217E expressed in 293T cells. (**B**) Quantification of the PLK1 and casein phosphorylation from (A), normalized relative to wild-type. Data are mean ± SE , N=3 independent experiments.* represents p=0.0005 (**C)** Experimental timeline for the synchronization of the PLK1 stable cell lines. (**D)** The mitotic index of parental HeLa T-rex cells transfected with control (GL2) or PLK1 siRNA or the stable PLK1 lines treated with PLK1 siRNA. DAta are mean ± SE, N=3 independent experiments with ≥ 100 cells counted per experiment. * represents p= 0.0001. (**E)** Percentage of cells in different stages of the mitotic cycle, treated as in D. Bars Bars are mean ± SE of ≥ 100 cells counted per experiment, N=3 independent experiments. (**F)** Immunofluorescence of cells fixed after treatment as in C. Fixed cells were stained with anti-BUBR1-pSer^{676} antibody (red), anti-BUBR1 antibody (green), and anti-CENPC antibody (blue) . Scale bar, 2 μm. Quantitation of the normalized BUBR1-pSer^{676} signal is shown. Data are mean ± SE of normalized signal from 15 cells with >30 kinetochores/cell, and are representative of 3 independent experiments. * represents p=0.0001.

Fig 6. Phosphotransferase activity of PLK1 Tyr^{217} mutants. (A) ΔT_m values for PLK1 proteins calculated upon ATP or kinase inhibitor incubations. Mean ΔT_m values ± SD (N=2) were calculated by subtracting the control T_m value (no ligand) from the measured T_m value. (**B)** PLK1 autophosphorylation and α-casein phosphorylation were visualized after autoradiography using [γ-^{32}P] ATP as co-factor (top panel). Equal loading of assayed protein was confirmed by Naphthalene blue staining of the nitrocellulose membrane (bottom 2 panels), N=2. **(C)** Activity of T210D (red),

T210D/Y217F (blue) and T210D/Y217E (black) PLK1 proteins measured in the presence of increasing concentrations of ATP using a direct fluorescent peptide-based kinase assay. Data are mean K_M values ± SD, N=2. (**D)** PLK1 in vitro kinase assays as in (**B)** but in the T210A PLK1 background, N=2. **(E)** PLK1 phosphotransfer activity towards an optimized PLK1 substrate peptide. Data are mean ± SD, (N=2). (**F)** MYC-PLK1 wild-type and mutants were expressed in 293T cells and immunoprecipitated before being resolved by SDS-PAGE and blotted for anti-PLK1-pThr^{210} antibody before being reprobed for MYC, (N=3).

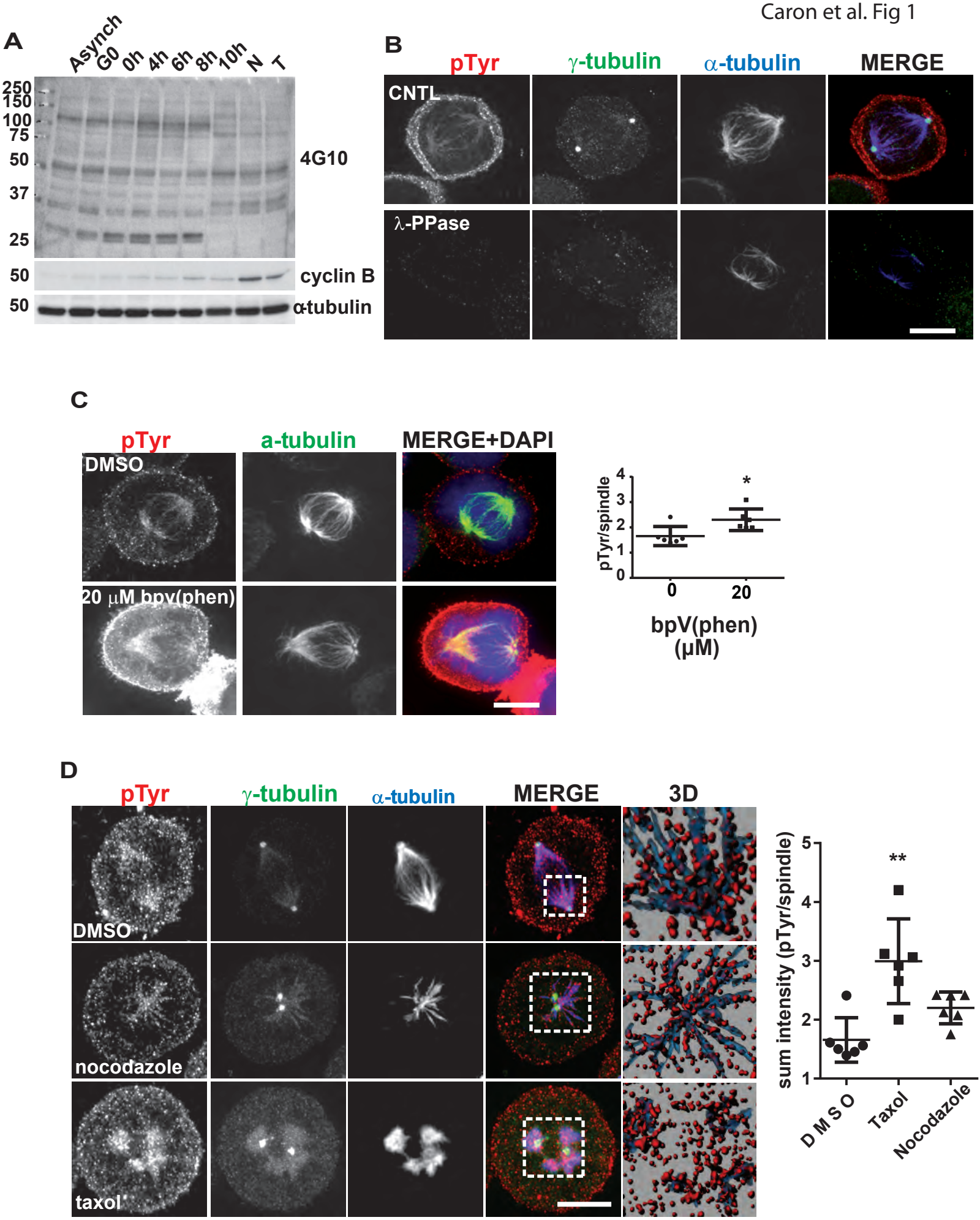
A
Asynch
G0
0h
4h
6h
8h
10h
N
T
250
150
100
75
50
37
25
4G10
50
cyclin B
50
α-tubulin
B
pTyr
γ-tubulin
α-tubulin
MERGE
CNTL
λ-PPase
C
pTyr
a-tubulin
MERGE+DAPI
DMSO
20 μM bpv(phen)
pTyr/spindle
0
1
2
3
4
*
0
20
bpV(phen)
(μM)
D
pTyr
γ-tubulin
α-tubulin
MERGE
3D
DMSO
nocodazole
taxol
sum intensity (pTyr/spindle)
1
2
3
4
5
**
D M S O
Taxol
Nocodazole

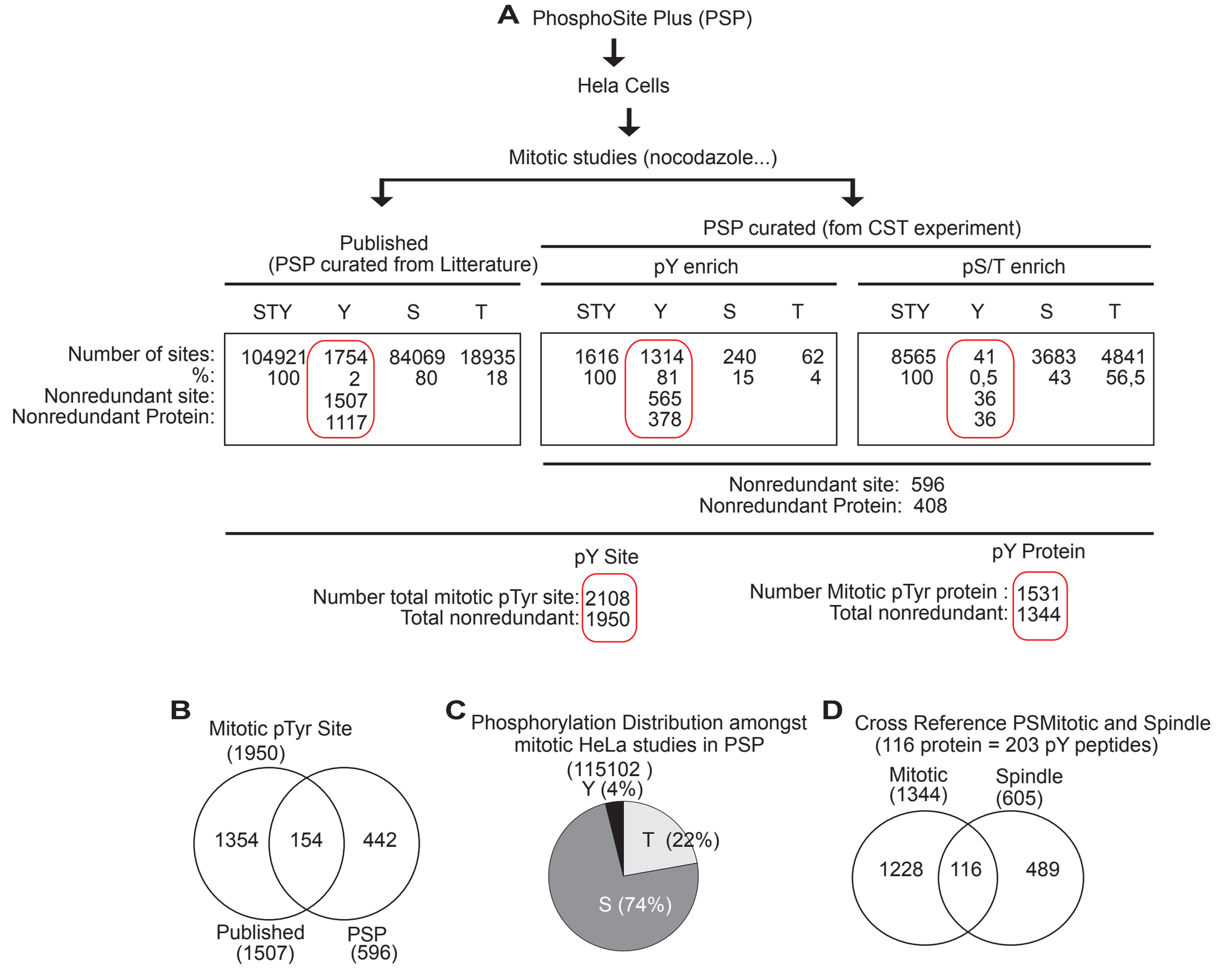
A
PhosphoSite Plus (PSP)
Hela Cells
Mitotic studies (nocodazole...)
Published
(PSP curated from Litterature)
PSP curated (fom CST experiment)
pY enrich
pS/T enrich
STY Y S T
STY Y S T
STY Y S T
Number of sites:
%:
Nonredundant site:
Nonredundant Protein:
104921 1754 84069 18935
100 2 80 18
1507
1117
1616 1314 240 62
100 81 15 4
565
378
8565 41 3683 4841
100 0,5 43 56,5
36
36
Nonredundant site: 596
Nonredundant Protein: 408
pY Site
Number total mitotic pTyr site: 2108
Total nonredundant: 1950
pY Protein
Number Mitotic pTyr protein : 1531
Total nonredundant: 1344
B
Mitotic pTyr Site
(1950)
1354
154
442
Published
(1507)
PSP
(596)
C
Phosphorylation Distribution amongst
mitotic HeLa studies in PSP
(115102)
Y (4%)
T (22%)
S (74%)
D
Cross Reference PSMitotic and Spindle
(116 protein = 203 pY peptides)
Mitotic
(1344)
Spindle
(605)
1228
116
489

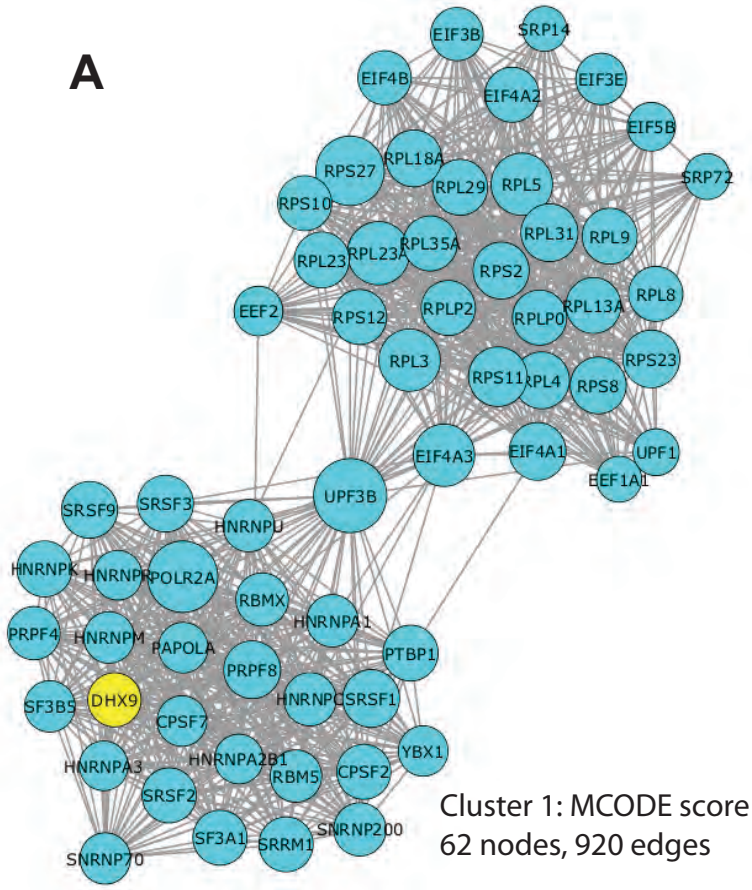

Cluster 1: MCODE score 30.16
62 nodes, 920 edges

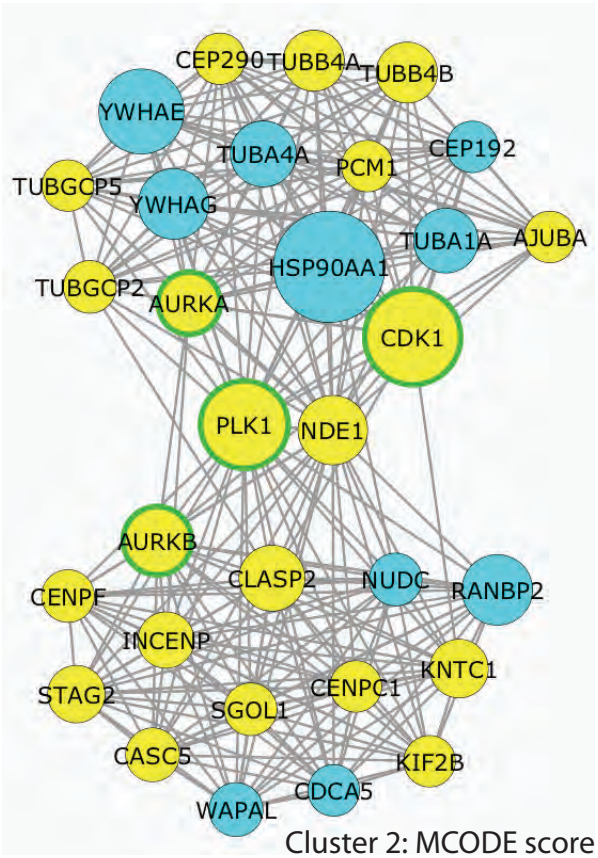

Cluster 2: MCODE score 17.20
31 nodes, 258 edges

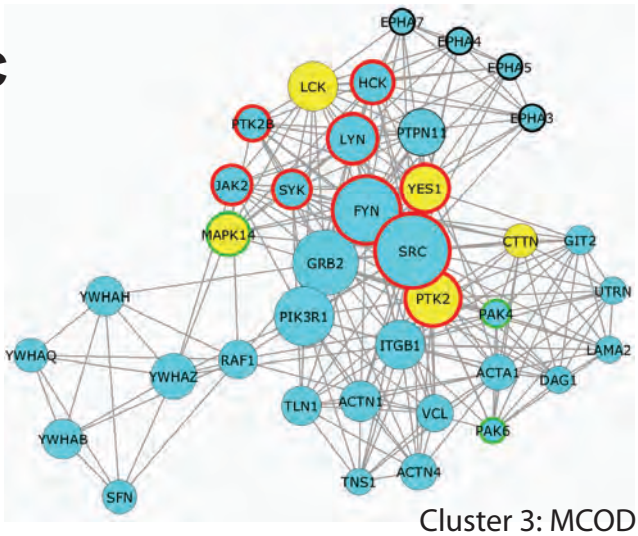

Cluster 3: MCODE score 13.35
38 nodes, 247 edges

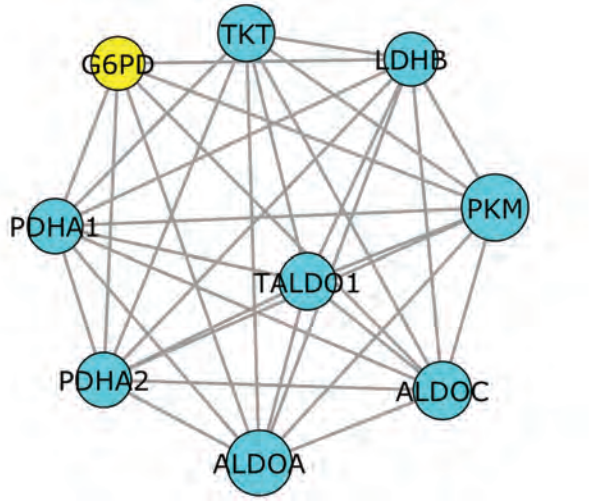

Cluster 4: MCODE score 8.50
9 nodes, 34 edges

Legend:

- Mitotic network
- Spindle subnetwork
- Tyr kinase
- Ser/Thr kinase
- Receptor Tyrosine kinase

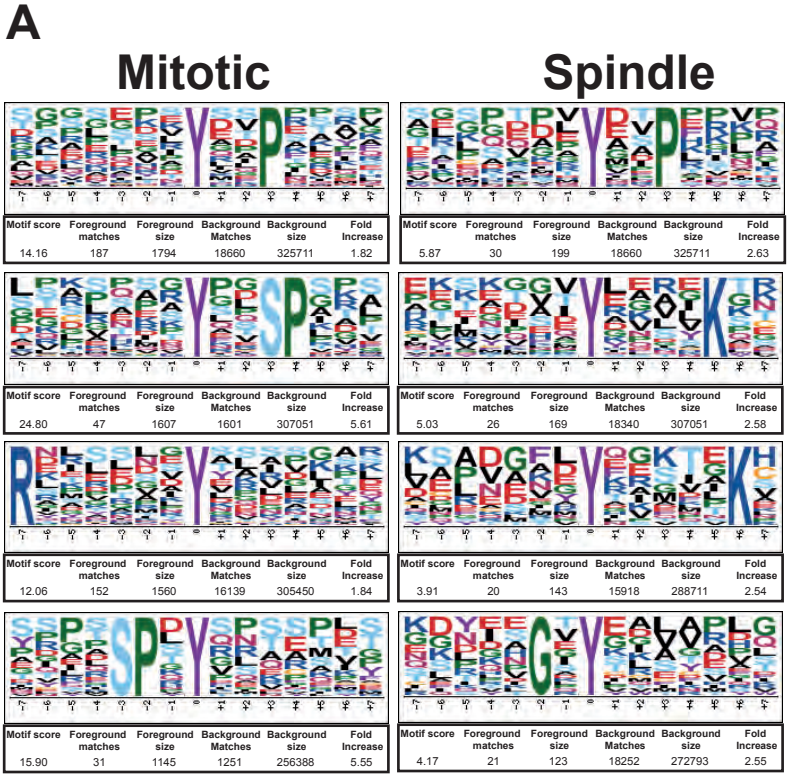
A
Mitotic
Spindle
Motif score | Foreground matches | Foreground size | Background Matches | Background size | Fold Increase
14.16 | 187 | 1794 | 18660 | 325711 | 1.82
5.87 | 30 | 199 | 18660 | 325711 | 2.63
24.80 | 47 | 1607 | 1601 | 307051 | 5.61
5.03 | 26 | 169 | 18340 | 307051 | 2.58
12.06 | 152 | 1560 | 16139 | 305450 | 1.84
3.91 | 20 | 143 | 15918 | 288711 | 2.54
15.90 | 31 | 1145 | 1251 | 256388 | 5.55
4.17 | 21 | 123 | 18252 | 272793 | 2.55

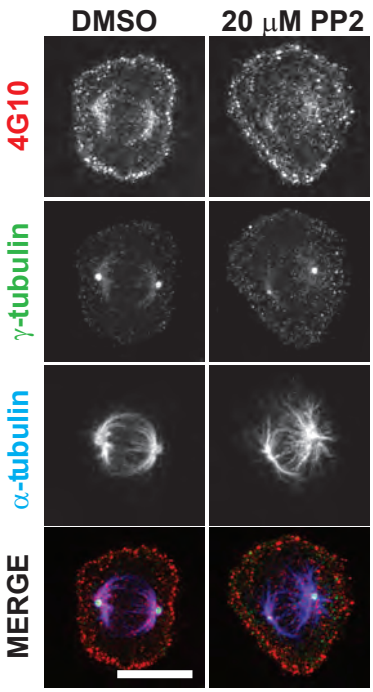
D
DMSO
20 μM PP2
4G10
γ-tubulin
α-tubulin
MERGE

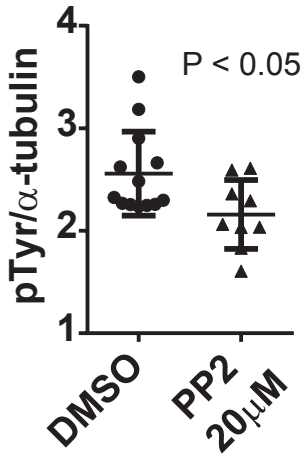
pTyr/α-tubulin
P < 0.05
DMSO
PP2 20μM

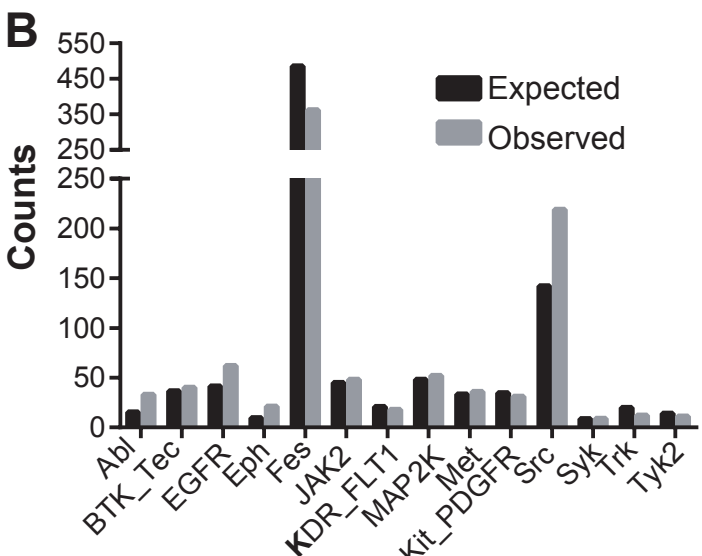
B
Counts
Expected
Observed
Abl
BTK_Tec
EGFR
Eph
Fes
JAK2
KDR_FLT1
MAP2K
Met
Kit_PDGFR
Src
Syk
Trk
Tyk2

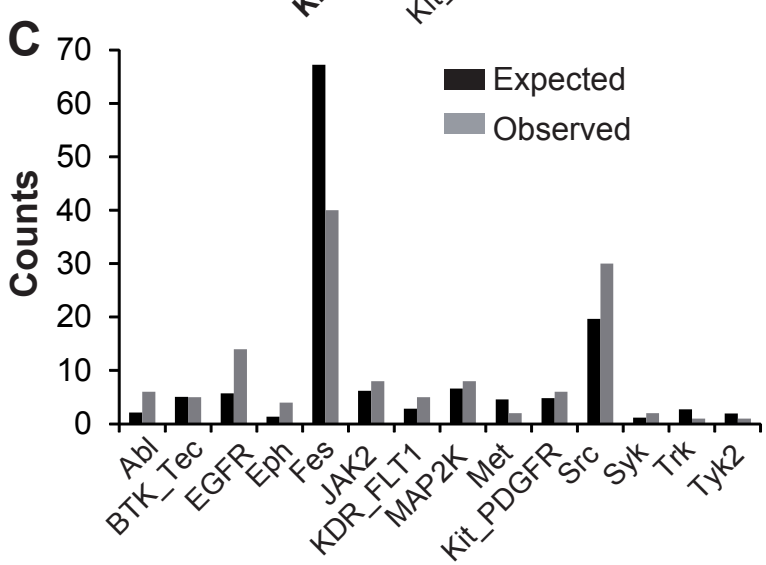
C
Counts
Expected
Observed
Abl
BTK_Tec
EGFR
Eph
Fes
JAK2
KDR_FLT1
MAP2K
Met
Kit_PDGFR
Src
Syk
Trk
Tyk2

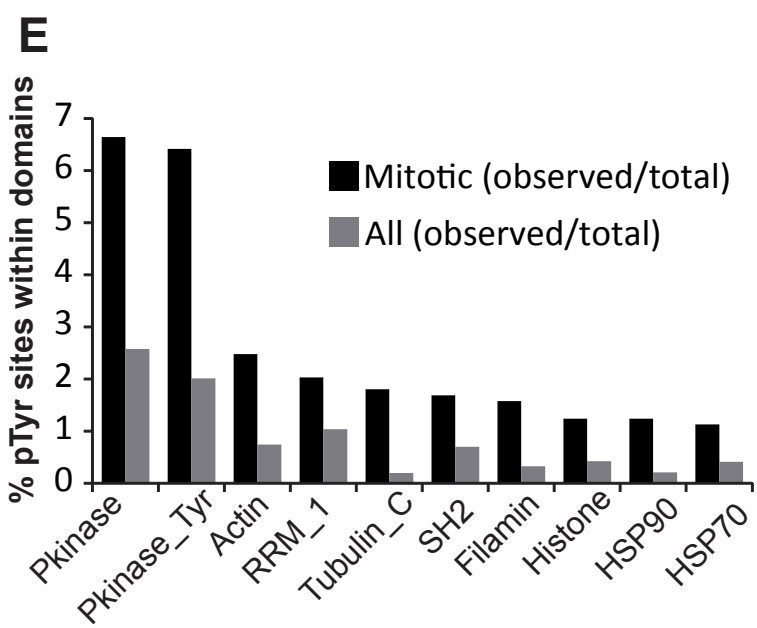
E
% pTyr sites within domains
Mitotic (observed/total)
All (observed/total)
Pkinase
Pkinase_Tyr
Actin
RRM_1
Tubulin_C
SH2
Filamin
Histone
HSP90
HSP70

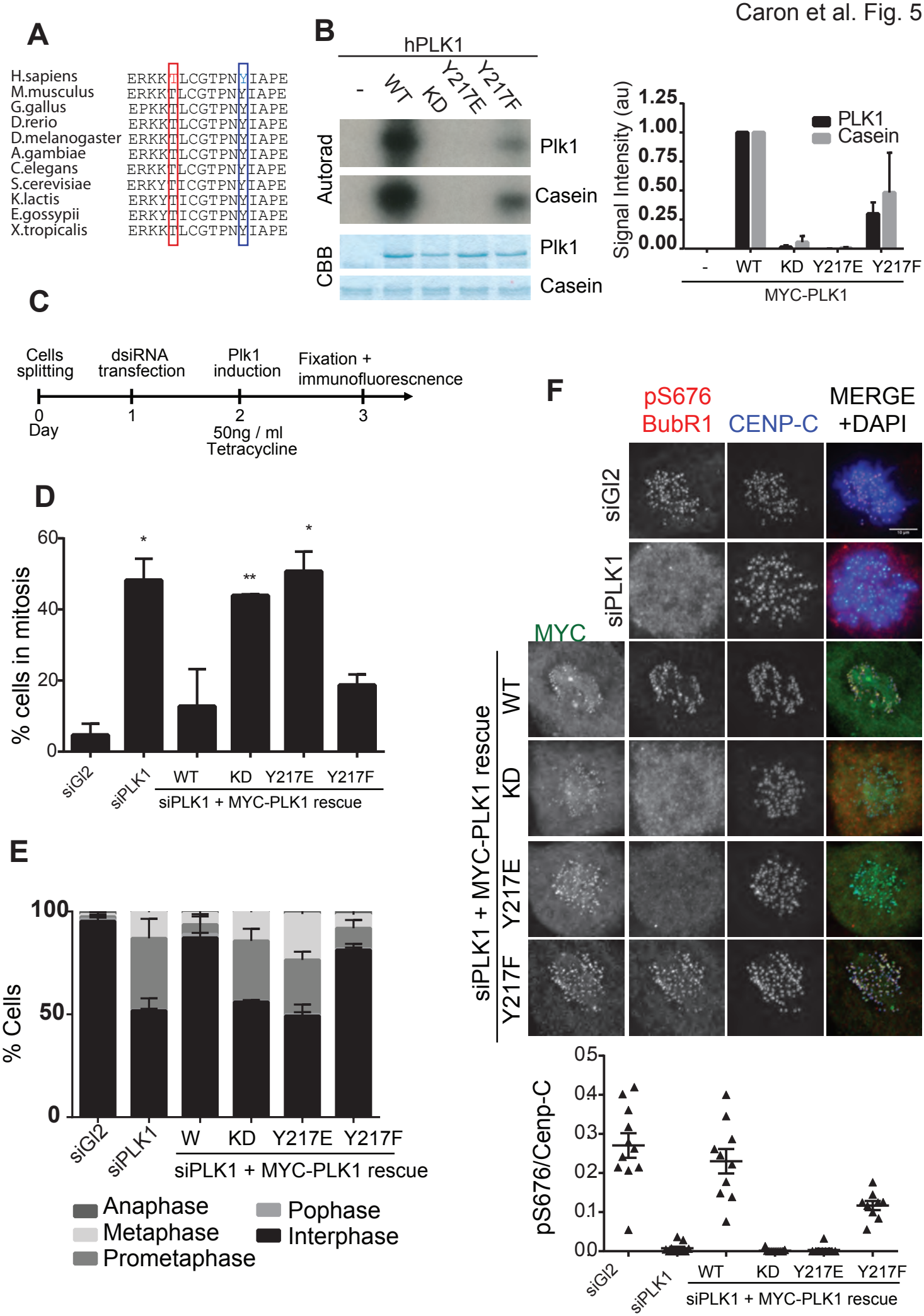
A
H.sapiens ERKKTLCGTPNYIAPE
M.musculus ERKKTLCGTPNYIAPE
G.gallus EPKKTLCGTPNYIAPE
D.rerio ERKKTLCGTPNYIAPE
D.melanogaster ERKKTLCGTPNYIAPE
A.gambiae ERKKTLCGTPNYIAPE
C.elegans ERKKTLCGTPNYIAPE
S.cerevisiae ERKYTICGTPNYIAPE
K.lactis ERKYTICGTPNYIAPE
E.gossypii ERKYTICGTPNYIAPE
X.tropicalis ERKKTLCGTPNYIAPE
B
hPLK1
-
WT
KD
Y217E
Y217F
Autorad
Plk1
Casein
CBB
Plk1
Casein
Signal Intensity (au)
1.25
1.00
0.75
0.50
0.25
0.00
PLK1
Casein
-
WT
KD
Y217E
Y217F
MYC-PLK1
C
Cells splitting
dsiRNA transfection
Plk1 induction
Fixation + immunofluorescnence
0
Day
1
2
50ng / ml Tetracycline
3
D
% cells in mitosis
60
40
20
0
*
**
*
siGl2
siPLK1
WT
KD
Y217E
Y217F
siPLK1 + MYC-PLK1 rescue
E
% Cells
100
50
0
siGl2
siPLK1
W
KD
Y217E
Y217F
siPLK1 + MYC-PLK1 rescue
Anaphase
Metaphase
Prometaphase
Pophase
Interphase
F
pS676 BubR1
CENP-C
MERGE +DAPI
siGl2
siPLK1
MYC
siPLK1 + MYC-PLK1 rescue
WT
KD
Y217E
Y217F
pS676/Cenp-C
05
04
03
02
0.1
00
siGl2
siPLK1
WT
KD
Y217E
Y217F
siPLK1 + MYC-PLK1 rescue

Caron et al. Fig 6.

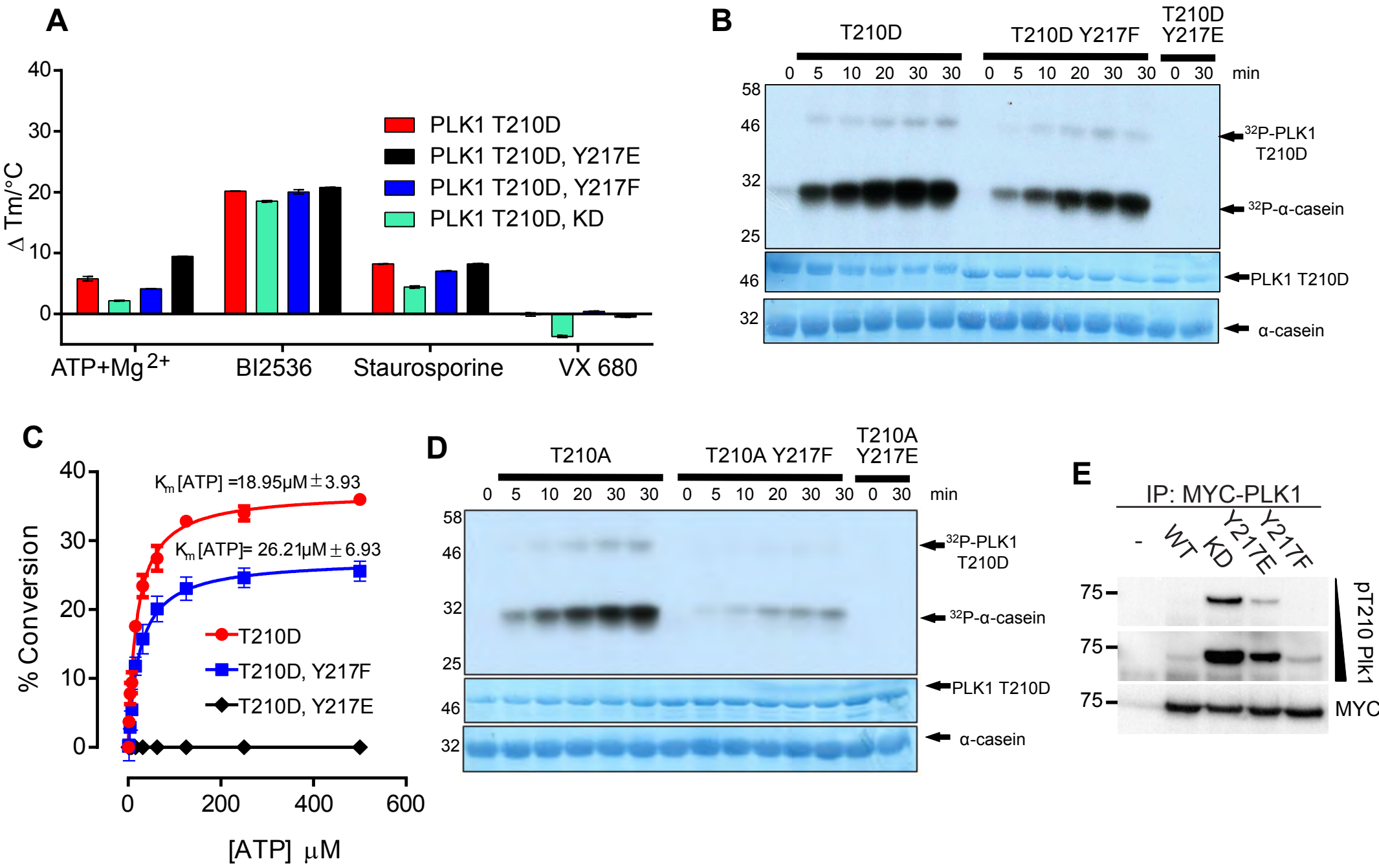

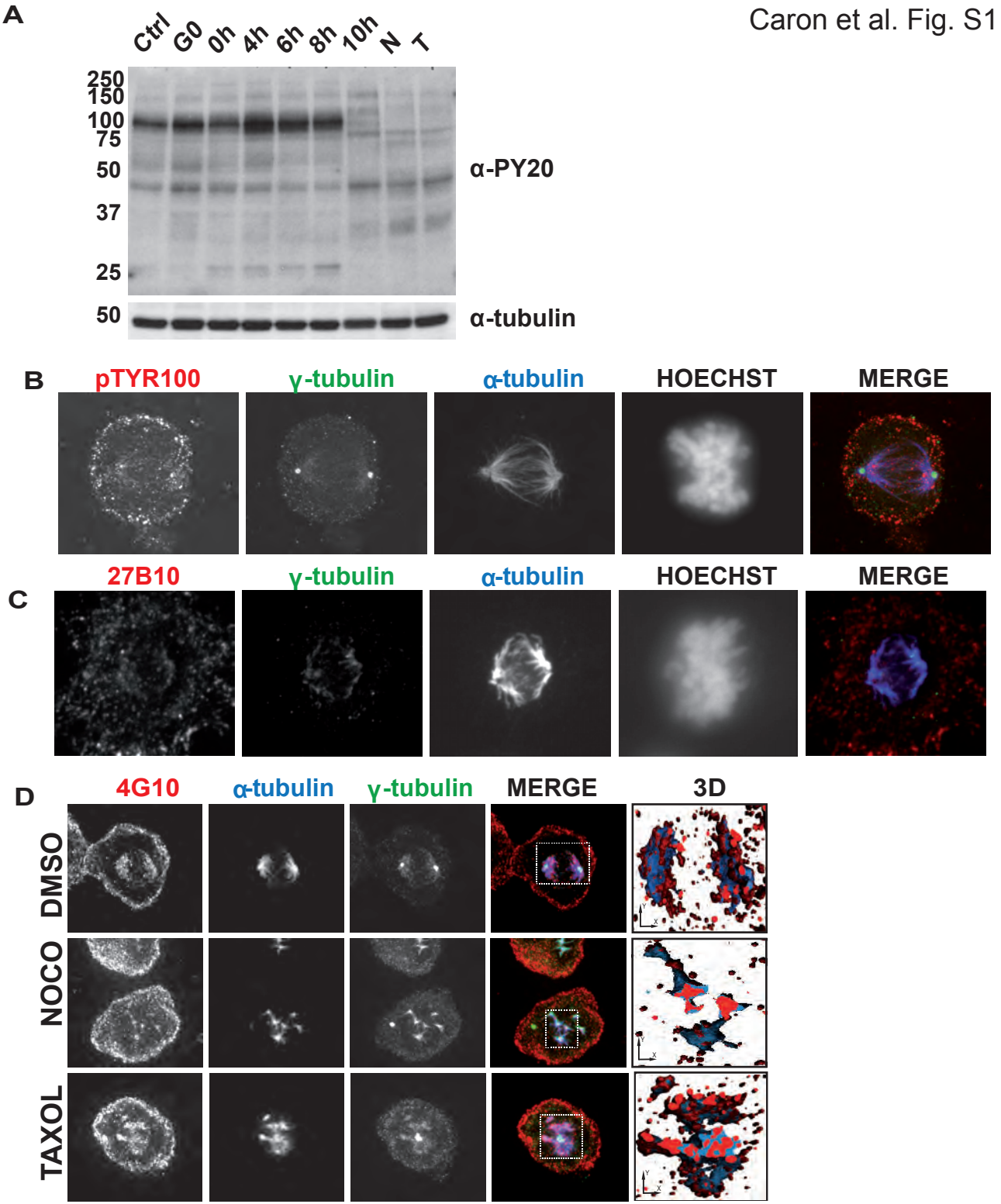
A
Ctrl
G0
0h
4h
6h
8h
10h
N
T
250
150
100
75
50
37
25
α-PY20
50
α-tubulin
B
pTYR100
γ-tubulin
α-tubulin
HOECHST
MERGE
C
27B10
γ-tubulin
α-tubulin
HOECHST
MERGE
D
4G10
α-tubulin
γ-tubulin
MERGE
3D
DMSO
NOCO
TAXOL

A

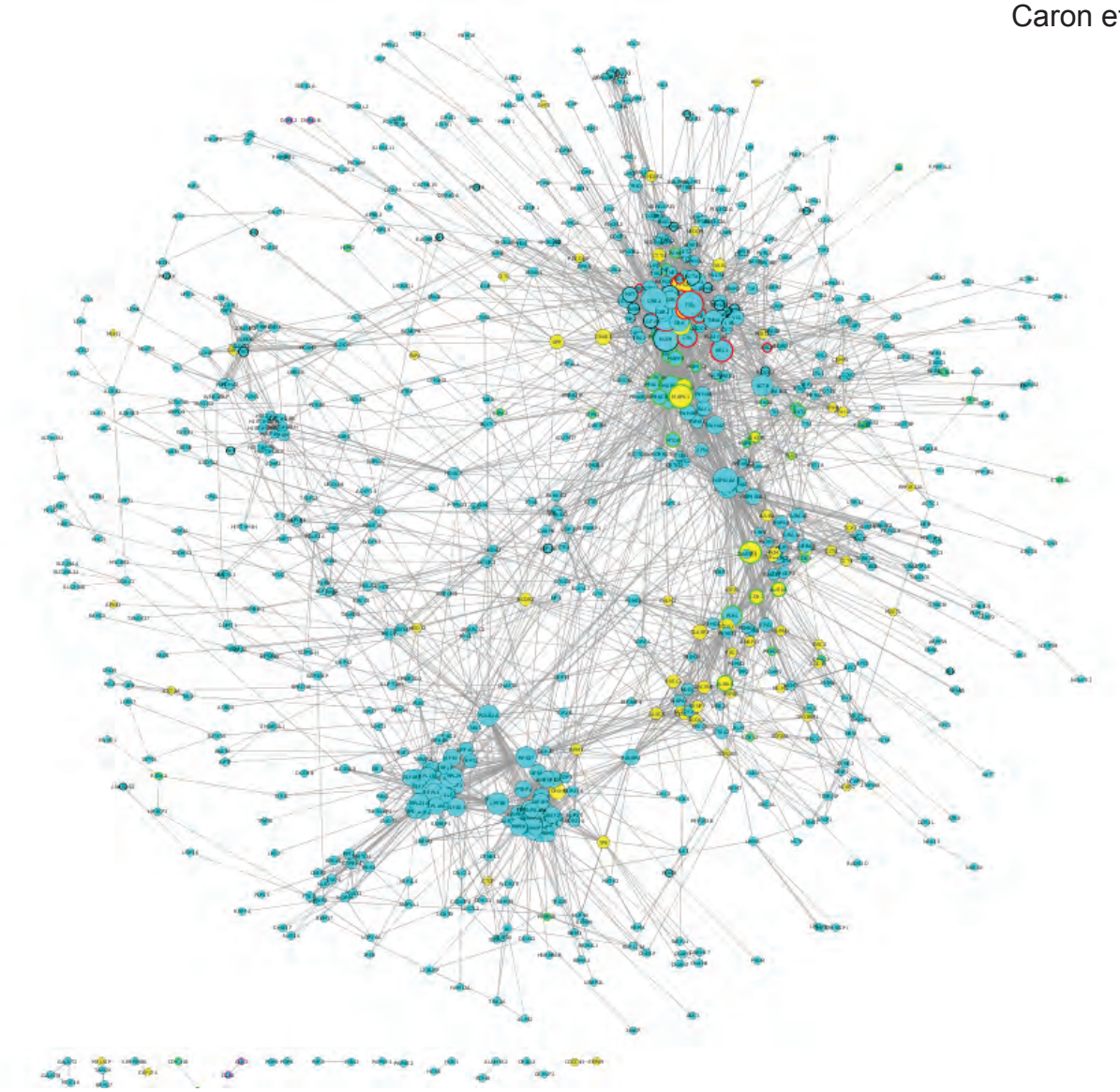

B

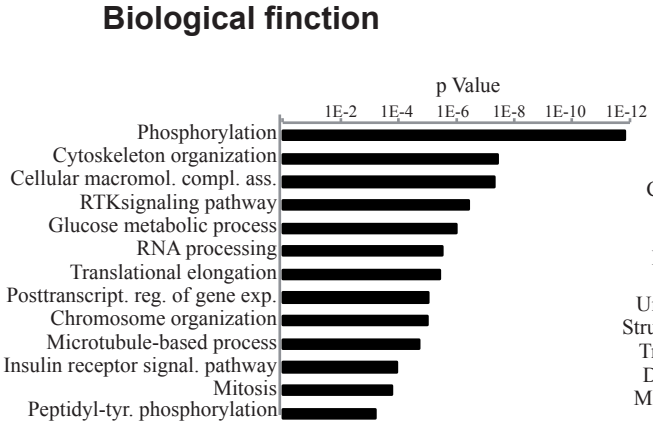
Biological finction
p Value
1E-2 1E-4 1E-6 1E-8 1E-10 1E-12
Phosphorylation
Cytoskeleton organization
Cellular macromol. compl. ass.
RTKsignaling pathway
Glucose metabolic process
RNA processing
Translational elongation
Posttranscript. reg. of gene exp.
Chromosome organization
Microtubule-based process
Insulin receptor signal. pathway
Mitosis
Peptidyl-tyr. phosphorylation

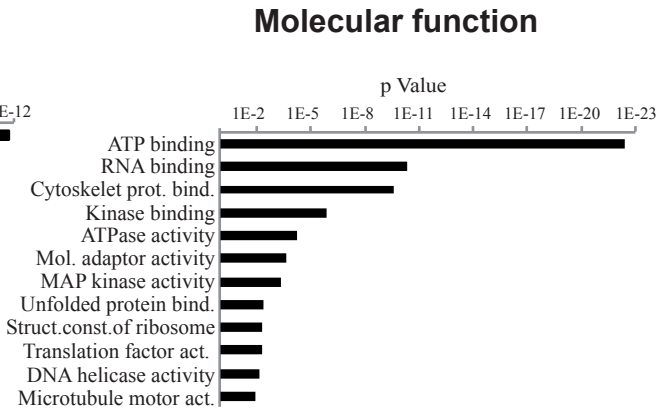
Molecular function
p Value
1E-2 1E-5 1E-8 1E-11 1E-14 1E-17 1E-20 1E-23
ATP binding
RNA binding
Cytoskelet prot. bind.
Kinase binding
ATPase activity
Mol. adaptor activity
MAP kinase activity
Unfolded protein bind.
Struct.const.of ribosome
Translation factor act.
DNA helicase activity
Microtubule motor act.

C

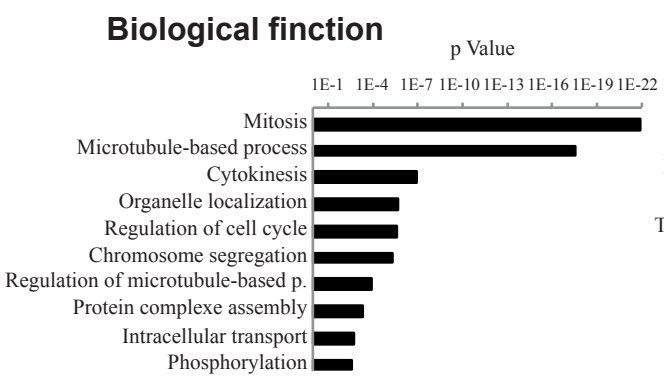
Biological finction
p Value
1E-1 1E-4 1E-7 1E-10 1E-13 1E-16 1E-19 1E-22
Mitosis
Microtubule-based process
Cytokinesis
Organelle localization
Regulation of cell cycle
Chromosome segregation
Regulation of microtubule-based p.
Protein complexe assembly
Intracellular transport
Phosphorylation

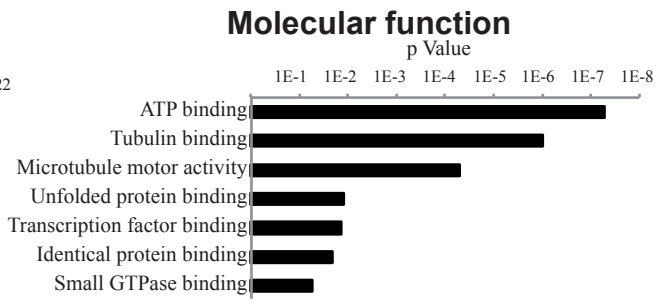
Molecular function
p Value
1E-1 1E-2 1E-3 1E-4 1E-5 1E-6 1E-7 1E-8
ATP binding
Tubulin binding
Microtubule motor activity
Unfolded protein binding
Transcription factor binding
Identical protein binding
Small GTPase binding

Caron et al. Fig. S3

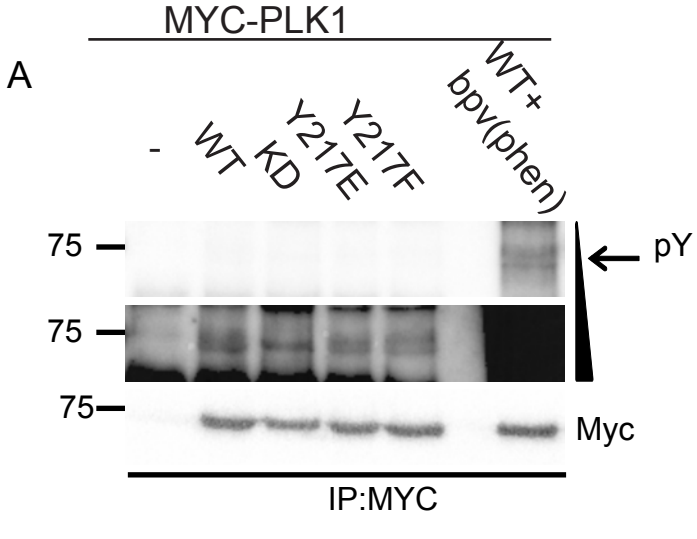

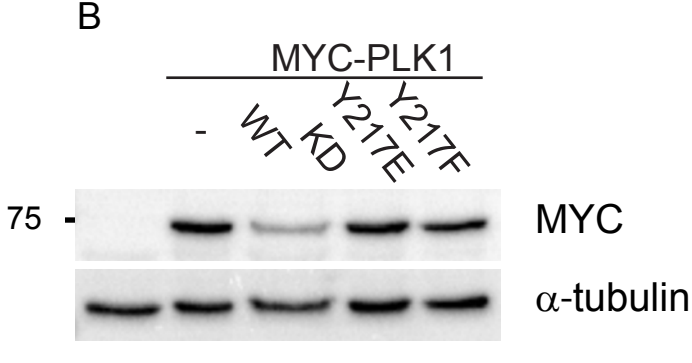

Caron et al. Fig. S4